



NWA 1152 and Sahara 00182: New primitive carbonaceous chondrites with affinities to the CR and CV groups

Caroline L. SMITH,^{1†} Sara S. RUSSELL,¹ Matthieu GOUNELLE,^{1,2}
Richard C. GREENWOOD,³ and Ian A. FRANCHI³

¹Department of Mineralogy, The Natural History Museum, Cromwell Road, London, SW7 5BD, UK

²Centre de Spectrométrie Nucléaire et de Spectrométrie de Masse, Université Paris 11, Bâtiment 104, 91405 Orsay Campus, France

³Planetary and Space Sciences Research Institute, The Open University, Walton Hall, Milton Keynes, Bucks, MK7 6AA, UK

[†]Present address: Division of Earth Sciences, Centre for Geosciences, University of Glasgow, Gregory Building, Lilybank Gardens, Glasgow, G12 8QQ, UK

*Corresponding author. E-mail: c.smith@earthsci.gla.ac.uk

(Received 10 September 2003; revision accepted 4 October 2004)

Abstract—We have investigated the mineralogy, petrography, bulk chemistry, and light element isotope composition of the ungrouped chondrites North West Africa (NWA) 1152 and Sahara 00182.

NWA 1152 contains predominantly type 1 porphyritic olivine (PO) and porphyritic olivine-pyroxene (POP) chondrules. Chondrule silicates are magnesium-rich ($\text{Fo}_{98.8 \pm 1.2}$, $n = 36$; $\text{Fs}_{2.3 \pm 2.1}$ $\text{Wo}_{1.2 \pm 0.3}$, $n = 23$). Matrix comprises ~40 vol% of the sample and is composed of a micron sized silicate groundmass with larger silicate, sulfide, magnetite, and Fe-Ni metal (Ni ~50 wt%) grains. Phyllosilicates were not observed in the matrix. Refractory inclusions are rare (0.3 vol%) and are spinel pyroxene aggregates or amoeboid olivine aggregates; melilite is absent from the refractory inclusions. Sahara 00182 contains predominantly type 1 PO chondrules, POP chondrules are less common. Most chondrules contain blebs of, and are often rimmed with, Fe-Ni metal and sulfide. Chondrule phenocrysts are magnesium-rich ($\text{Fo}_{92.2 \pm 0.6}$, $n = 129$; $\text{Fs}_{4.4 \pm 1.8}$ $\text{Wo}_{1.3 \pm 1.1}$, $n = 16$). Matrix comprises ~30 vol% of the meteorite and is predominantly sub-micron silicates, with rare larger silicate grains. Matrix Fe-Ni metal (mean Ni = 5.8 wt%) and sulfide grains are up to mm scale. No phyllosilicates were observed in the matrix. Refractory inclusions are rare (1.1 vol%) and melilite is absent. The oxygen isotope composition of NWA 1152 falls within the range of the CV chondrites with $\delta^{17}\text{O} = -3.43\text{‰}$ $\delta^{18}\text{O} = 0.70\text{‰}$ and is similar to Sahara 00182, $\delta^{17}\text{O} = -3.89\text{‰}$, $\delta^{18}\text{O} = -0.19\text{‰}$ (Grossman and Zipfel 2001).

Based on mineralogical and petrographic characteristics, we suggest NWA 1152 and Sahara 00182 show many similarities with the CR chondrites, however, oxygen isotopes suggest affinity with the CVs. Thus, neither sample can be assigned to any of the currently known carbonaceous chondrite groups based on traditionally recognized characteristics. Both samples demonstrate the complexity of inter- and intra-group relationships of the carbonaceous chondrites. Whatever their classification, NWA 1152 and Sahara 00182 represent a source of relatively pristine solar system material.

INTRODUCTION

Among the five chondrite classes (carbonaceous, ordinary, enstatite, Rumuruti-like, and Kakangari-like), the carbonaceous chondrites account for the greatest diversity in chemical composition and texture. Although these meteorites have been extensively studied, the relationships among and between the carbonaceous chondrite groups are often obscure. Recent finds from Antarctica and the hot deserts have greatly increased the number of carbonaceous chondrite samples within our collections. Correspondingly, the chemical,

mineralogical, and petrographic characteristics of recognized carbonaceous chondrites have become more diverse, with the result that many samples may not easily be assigned to one of the traditionally recognized classes. For example, the Antarctic meteorites MacAlpine Hills (MAC) 87300 and MAC 88107 appear to be intermediate between CM and CO meteorites on the basis of elemental abundance and CAI mineralogy, suggesting a link between these classes (Russell et al. 2000). Likewise, the unusual carbonaceous chondrite Tagish Lake shows characteristics similar to both the CI and CM groups on the basis of light element geochemistry (Grady

et al. 2002) and overall element abundance patterns (Mittlefehldt 2002), although in terms of its mineralogy and petrography, it cannot be allied with either the CIs or the CMs (Zolensky et al. 2002). The carbonaceous chondrite Acfer 094 is believed to be unique though it shows some similarities with the both the CO and CM chondrites; the chemical composition and abundance of certain chondrule types suggests affinity with the CMs, whereas the lack of phyllosilicates and the oxygen isotope composition is more consistent with a CO3 classification (Newton et al. 1995).

Several workers have attempted to estimate the number of parent bodies required to supply the total known range of carbonaceous chondrites and to determine genetic links between them using the oxygen three-isotope system. Clayton and co-workers initially suggested that oxygen isotopes can be used to indicate asteroidal sources—samples with different bulk $\Delta^{17}\text{O}$ values being likely to originate on different parent bodies (Clayton 1999). However, this picture is complicated by the models of Clayton and Mayeda (1984) and Young et al. (1999) who have shown that the differences in bulk $\Delta^{17}\text{O}$ can plausibly be accounted for by differences in the degree of aqueous alteration, provided that the water and rock sources have distinguishable oxygen isotope compositions.

We have characterized the mineralogy and petrography of the unusual carbonaceous chondrites North West Africa (NWA) 1152 and Sahara 00182. The aims of this study were: 1) to classify these meteorites and, 2) to establish their relationship to other carbonaceous chondrites, with the aim of casting light on the types and number of carbonaceous chondrite parent bodies, the nature of the alteration events they experienced, and the likelihood of genetic links between different groups.

SAMPLES AND TECHNIQUES

NWA 1152 is a single stone of 98 g that was recovered along the Morocco/Algerian border in 1999. The stone was purchased in Tagounite by Monsieur B. Fectay. Sahara 00182 is a single stone of 70 g collected in 2000 and it is listed in *The Meteoritical Bulletin* (2001) as an ungrouped C3 meteorite. The thin section analyzed here is from the Institut für Planetologie, Münster.

Mineralogical and Petrologic Analyses

Thin and thick sections of NWA 1152 (thick section nr. P11463; thin section nr. P11582) and the thin section of Sahara 00182 (PL00110) were examined using an optical microscope in both transmitted and reflected light. Compositions of silicate mineral and metal phases within chondrules and large grains within the matrix were determined by EPMA on the Cameca SX50 electron microprobe at the Natural History Museum (London) in WDS (wavelength dispersive spectroscopy) mode using appropriate silicate and metal standards. Operating conditions were a 15 keV accelerating

voltage, with a 20 nA beam current and a $\sim 1\ \mu\text{m}$ diameter spot. Data were reduced using the protocol of Bence and Albee (1968). Bulk composition of matrix material was determined on the Cameca SX50 using a 40 μm defocused beam, 15 keV accelerating voltage, and a beam current of 20 nA. On-line corrections are applied automatically for spectrometer angles, count times, crystal selection, specimen movement, and PAP corrections. Detection limits are shown in Table 2.

Modal abundance analyses of different components (chondrule, refractory inclusion, opaque, matrix) within NWA 1152 and Sahara 00182 were carried out by image analyses of high-resolution BSE images and X-ray elemental maps. Images were analyzed using the Adobe® Photoshop® computer program. A thin section of Renazzo was analyzed using this method to compare with literature data obtained using the traditional transmitted and reflected light microscopy method by point counting.

Light Element Stable Isotope Analyses

Carbon, nitrogen, and oxygen isotope analyses of NWA 1152 and carbon and nitrogen analyses of Sahara 00182 were carried out at the Open University on powdered and homogenized sub-samples.

Carbon isotope analyses were carried out using a PDZ Europa Ltd. *Geo 20/20* continuous flow/dual-inlet mass spectrometer. Samples are combusted at 1200 °C in the presence of oxygen (produced from CuO) converting carbon to the gaseous species CO_2 and the isotopic composition ($\delta^{13}\text{C}$) measured relative to PDB. Samples containing at least 1 μg of carbon may be analyzed to a precision of 0.1‰ or better (Smith 2002).

Nitrogen isotope compositions were measured on the *Finesse* multi-collector, high-precision, static vacuum, mass spectrometer, designed and built at the Open University (Verchovsky et al. 1997, 1998). Nitrogen isotopes ($\delta^{15}\text{N}$) are measured relative to AIR and can be measured to a precision of 1.0‰, with a minimum N content of 1 ng.

High-precision oxygen stable isotope analyses were carried out using a combination of IR-laser fluorination and mass spectrometry as described by Miller et al. (1999). For 0.5–2.0 mg of silicate and oxide samples the analytical precision is typically 0.08 and 0.04‰, for $\delta^{18}\text{O}$ and $\delta^{17}\text{O}$ respectively (Miller et al. 1999).

Chemical Analyses

Sample chips were taken from NWA 1152 and Sahara 00182 from internal portions, thus avoiding surface weathering and fusion crust.

Bulk major and minor elemental analyses were carried out using a Varian *Vista Pro* ICP-AES at the Natural History Museum. Two 50 mg powdered sub-samples were taken from 254 mg of NWA 1152 and 181 mg of Sahara 00182. These

sub-samples were then fused with 300 mg LiBO_2 in Pt/Au crucibles (Thompson and Walsh 1983). The fused samples were dissolved in 1M HNO_3 (Aristar grade) and made up to 250 ml. Allende reference material (Allende Split 19/Position 11; Jarosewich et al. 1987) and BCR-1 were analyzed as secondary standards and the instrument was calibrated with synthetic standards.

DESCRIPTION OF NWA 1152

NWA 1152 has a clearly chondritic texture, with well-defined chondrules ranging in size between approximately 250 μm and 2 mm in diameter (Fig. 1). The modal abundance of different components within NWA 1152 are listed in Table 1.

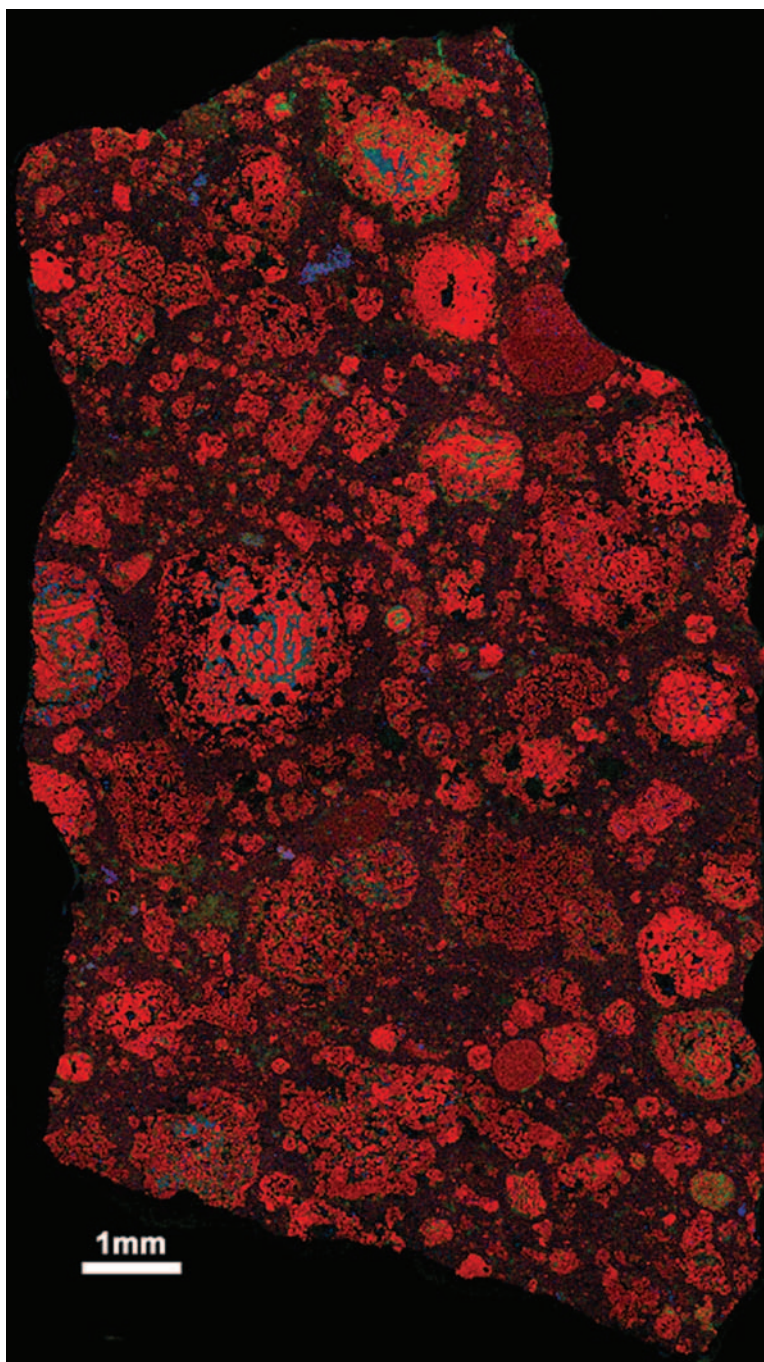


Fig. 1. X-ray elemental map of NWA 1152 showing the distribution of chondrules, matrix, and refractory inclusions; red = Mg, blue = Al, and green = Ca.

Table 1. Modal abundances of petrographic features within NWA 1152 and Sahara 00182.^a

	NWA 1152	Sahara 00182	Renazzo ^b	Renazzo ^c	CRs ^d	CVs ^e
Chondrules + chondrule fragments (vol%)	52.2	64.9	51.1	54.0	37.0–63.1	33.0–52.5
Chondrule apparent diameter (mean, mm)	0.90	1.01	0.86	0.83	0.7	1.0
Opaque phases ^f (vol%)	4.1	6.9	6.1	8.1	4.8–10.2	3.1–4.8
Matrix ^g (vol%)	42.8	27.6	41.9	45	29.7–63.0	34.5–51.3
Refractory inclusions (vol%)	0.3	1.1	0.9	1.0	0.1–2.6	6.1–11.5
Matrix/chondrule ratio	0.82	0.43	0.82	0.83	0.60–1.85	0.55–1.17

^aAbundances from CR and CV samples are also shown for comparison.^bThis study.^cData from Weisberg et al. (1993).^dData from Weisberg et al. (1993) and Kallemeyn et al. (1994).^eData from McSween (1977), Grossman et al. (1988), and Rubin (2000).^fIncludes opaque phases in chondrules and isolated opaques within matrix.^gIncludes fine-grained silicates and microfragments.Table 2. Representative analyses of silicate and opaque phases within chondrules in NWA 1152.^a

	Silicate Grams			Pyroxene			Mesostasis		
	Olivine								
Na ₂ O	bd	bd	bd	bd	bd	bd	0.06	bd	bd
MgO	55.71	57.34	56.95	39.28	39.09	38.40	24.57	17.78	19.64
Al ₂ O ₃	0.04	0.24	0.08	0.77	0.74	0.30	11.49	8.26	3.91
SiO ₂	40.99	41.40	41.49	57.81	58.37	58.11	44.80	49.42	51.27
CaO	0.24	0.30	0.25	0.62	0.74	0.52	17.52	22.45	24.08
TiO ₂	bd	0.09	bd	0.13	0.20	0.07	0.26	1.68	0.13
Cr ₂ O ₃	0.24	0.15	0.18	0.41	0.76	0.71	0.15	0.49	0.14
MnO	0.19	0.03	0.10	0.05	0.23	0.10	0.05	0.12	0.04
FeO	2.73	0.47	0.80	0.63	1.01	1.53	0.29	0.54	0.42
Total	100.14	100.02	99.85	99.7	101.14	99.74	99.19	100.74	99.63
	Fo 97.3	Fo 99.5	Fo 99.2	Fs 0.9	Fs 1.4	Fs 2.2	Fs 0.4	Fs 0.9	Fs 0.6

Opaque phases

Fe-Ni metal in olivine

	Sulfides in rim		
Si	0.04	0.04	0.05
P	bd	bd	bd
S	0.02	bd	0.03
Ti	0.02	0.02	bd
Cr	0.11	0.07	0.06
Fe	94.21	94.32	95.13
Co	0.24	0.45	0.34
Ni	5.07	5.06	4.60
Total	99.72	99.97	100.21
			35.82
			0.03
			bd
			0.02
			bd
			bd
			63.31
			0.06
			0.07
			99.09
			98.96

^aDetection limits (wt% oxide): Na = 0.06, Mg = 0.02, Al = 0.04, Si = 0.02, P = 0.04, S = 0.02, Cl = 0.02, K = 0.03, Ca = 0.02, Ti = 0.02, Cr = 0.04, Mn = 0.03, Fe = 0.03, Ni = 0.03, Co = 0.03, P₂O₅, Cl, and K₂O were all below detection limits in silicate phases, Mn was below detection in sulfide and metal phases.

Chondrules

The majority of chondrules are irregularly shaped and many are fragmented. Type 1 PO chondrules dominate the sample, some POP chondrules also occur. Rare cryptocrystalline chondrules can be also seen. Olivine within the chondrules is extremely MgO-rich with a mean composition of $Fo_{98.8 \pm 1.2}$ (1σ) ($n = 36$, range 94.3–99.7), CaO contents range between 0.06–0.67 wt%, with a mean content of 0.31 wt%. Occasionally, small blebs of Fe-Ni metal up to approximately 20 μm in size occur within olivine grains. Ni in these blebs ranges between 4.0 and 8.0 wt%. Pyroxene within the chondrules is predominantly low-Ca and is also MgO-rich with a mean composition of $Fs_{2.3 \pm 2.1}$ (1σ), $Wo_{1.2 \pm 0.33}$ (1σ), ($n = 23$, Fs range 0.82–8.6). The most abundant type of mesostasis is Ca- and Al-rich (CaO 9.5–24.7 wt%; Al_2O_3 2.8–37.4 wt%) and crystalline, although in some chondrules is glassy. Many of the chondrules exhibit layering with cores of POP, PO, or occasionally BO texture surrounded, or partly surrounded, by blebs of predominantly sulfide and magnetite with rare Fe-Ni metal. Often the sulfide/magnetite rim is itself surrounded by a rim of fine-grained forsteritic olivine and low-Ca pyroxene (Figs. 2a and 2b). However, much of the sulfide and magnetite (and occasional Fe-Ni metal) is oxidized to iron hydroxide. This oxidation is due to terrestrial weathering and the sample is weathering grade 2 (Wlotzka 1993). Magnetite

and sulfide veins and veinlets also crosscut the main body and the fine-grained rims around the chondrules. These veins appear to be a feature of secondary alteration on the parent body. Some terrestrial carbonate veining can also be seen running through the sample. Representative compositions of olivines, pyroxenes, Fe-Ni metal, and sulfides within NWA 1152 chondrules are given in Table 2.

Matrix

Matrix within NWA 1152 is composed of a groundmass of granular (micron-scale) silicates with larger (up to $\sim 75 \mu\text{m}$) angular to irregular shaped silicate, Fe-Ni metal, sulfide, and magnetite grains (Figs. 3a and 3b). Phyllosilicates are not observed within the matrix indicating that NWA 1152 is petrologic type 3 (Van Schmus and Wood 1967). Larger olivine grains within the matrix range in size between ~ 10 – $75 \mu\text{m}$ and are similar in composition to the chondrules, with a mean composition of $Fo_{95.4 \pm 1.2}$ (1σ) and mean CaO of 0.22 wt%. Some larger grains of low-Ca pyroxene occur and rarer diopside ($Fs_{0.8 \pm 0.3}$ [1σ], $Wo_{48.8 \pm 2.7}$ [1σ]) is also present. Representative compositions of silicate grains within matrix are given in Table 3 and bulk matrix analyses by broad, defocused electron beam (40 μm diameter) are shown in Table 4a. The low totals in the defocused beam analyses (our data and that of McSween and

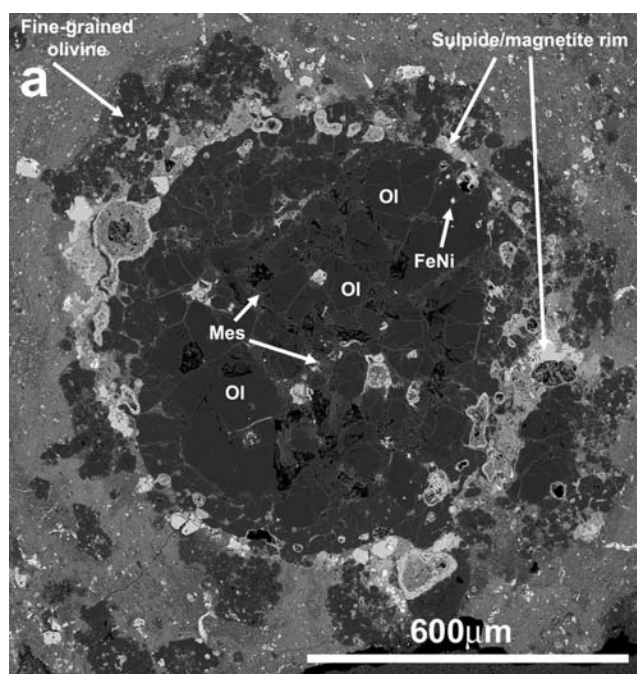


Fig. 2a. A BSE image of a porphyritic olivine chondrule in NWA 1152. The chondrule is dominated by olivine grains tens to $\sim 100 \mu\text{m}$ in size, with crystalline Ca-Al-rich mesostasis (light grey). Some small (few microns) blebs of Fe-Ni metal occur in the chondrule olivine. Partly surrounding the chondrule is a rim composed of sulfide (light grey) and magnetite (darker grey). This rim itself has been altered due to terrestrial weathering forming iron hydroxides. In some areas, masses of fine-grained olivine adhere to the sulfide-magnetite rim material.

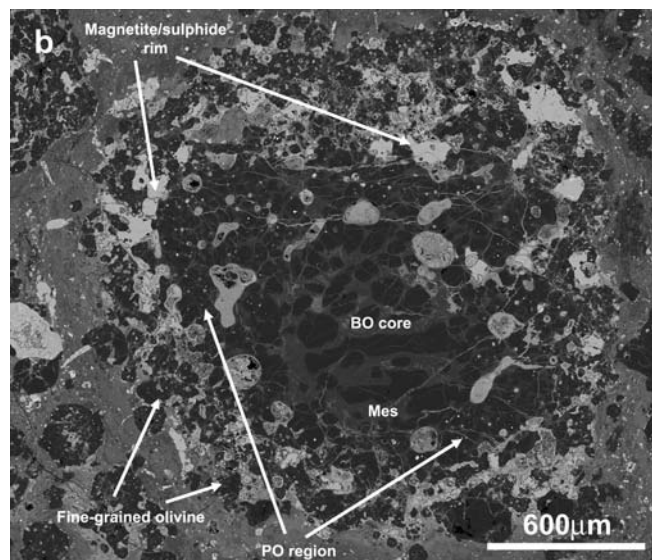


Fig. 2b. A BSE image of a barred olivine/porphyritic olivine chondrule in NWA 1152. The center region displays barred olivine morphology, with a very fine crystalline Ca-Al mesostasis. Fe-Ni metal blebs cannot be seen in olivine in the BO core. Around the core BO region is an incomplete rim of globular masses composed primarily of iron oxides with some magnetite. These may have been formed through nebular alteration of primary metals and/or sulfides. Completely surrounding the BO core is a region displaying PO morphology, with Ca-Al crystalline mesostasis. Fe-Ni metal blebs can be seen in olivine grains within the PO region. Partly surrounding the PO region is a rim of sulfide and magnetite, some of which has been altered to iron hydroxide. Similar to Fig. 2b, fine-grained olivine masses can be seen adhering to the sulfide-magnetite rim.

Table 3. Representative analyses of silicate grains and isolated opaque phase within matrix in NWA 1152.^a

Silicate grains									
	Olivine			Low-Ca pyroxene			Diopside		
Na ₂ O	bd	bd	bd	bd	bd	bd	bd	bd	bd
MgO	54.08	53.98	53.51	36.32	38.17	35.60	17.78	19.64	20.21
Al ₂ O ₃	bd	0.06	bd	1.23	0.19	3.10	8.26	3.91	2.77
SiO ₂	40.95	41.49	40.79	55.43	58.42	54.71	49.42	51.27	52.58
P ₂ O ₅	bd	bd	bd	bd	bd	0.10	bd	bd	bd
CaO	0.19	0.19	0.19	0.84	0.16	1.22	22.45	24.08	23.77
TiO ₂	bd	bd	bd	0.10	0.05	0.17	1.68	0.13	0.21
Cr ₂ O ₃	0.07	0.20	0.32	0.50	0.42	0.51	0.49	0.14	bd
MnO	0.44	0.27	0.19	0.21	0.16	0.15	0.12	bd	0.05
FeO	4.74	4.48	4.65	5.08	3.30	4.41	0.54	0.42	0.40
Total	100.47	100.67	99.65	99.71	100.87	99.97	100.74	99.59	99.99
	Fo 95.3	Fo 95.6	Fo 95.4	Fs 7.2	Fs 4.6	Fs 6.4	Fs 0.9	Fs 0.6	Fs 0.6

Opaque phases						
	Fe-Ni Metal grains			Sulfide grains		
Si	0.03	bd	bd	bd	bd	0.05
S	bd	bd	bd	35.89	35.55	35.75
Ti	0.02	bd	bd	bd	bd	bd
Fe	42.53	90.65	49.82	63.21	64.30	63.12
Co	1.89	3.76	0.79	0.07	bd	bd
Ni	55.72	6.11	49.92	0.18	bd	0.12
Total	100.18	100.52	100.53	99.35	99.85	99.04

^aCl and K₂O were below detection limits in the silicate phases. P, Cr, and Mn were below detection in the metal and sulfide phases.

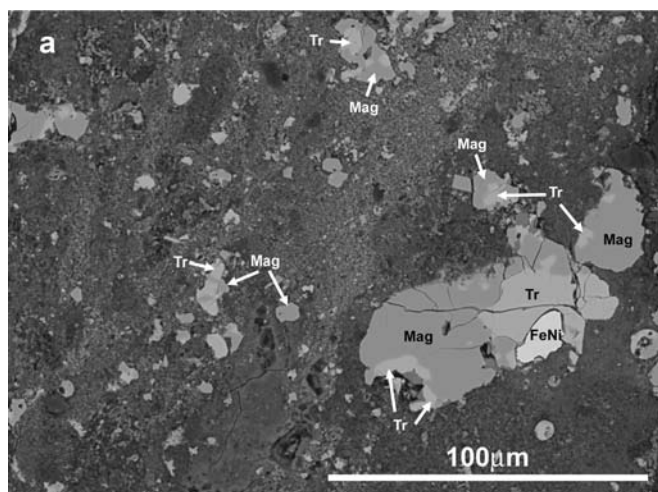


Fig. 3a. A BSE image of typical matrix within NWA 1152. Prominent masses of Fe-Ni metal, sulfide, and magnetite can be seen, ranging from tens of microns to ~100 μm in size. Some grains of olivine can also be seen (~10–20 μm) in the granular groundmass of the matrix.

Richardson [1977]) is likely due to the presence of voids and surface roughness. Si normalized matrix analyses are shown in Table 4b.

Isolated Opaques

Approximately 2 vol% of the meteorite is composed of Fe-Ni metal, magnetite, and troilite grains, which are often quite angular and range in size between 10–40 μm. Similar to

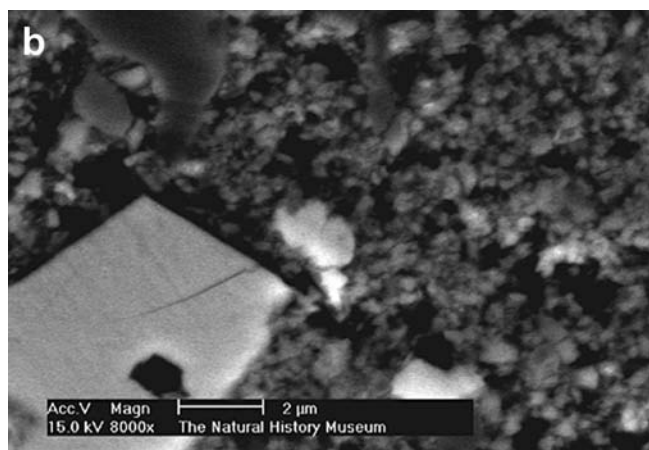


Fig. 3b. A high-resolution BSE image of matrix within NWA 1152. This image clearly shows the granular nature of the silicate matrix groundmass. A larger olivine grain, with a ferroan rim, can be seen in the top left of the image. At the bottom left of the image is an angular grain of magnetite.

the chondrules, sulfide is the dominant phase, although approximately a third of the matrix opaque grains are Fe-Ni metal. Fe-Ni metal matrix grains occur as two types; the dominant type is tetrataenite, characterized by high Ni contents (mean 50.2 wt%, range 46.4–55.7 wt%), the second type is kamacite, which is less common and is characterized by high Co abundance (3.1–11.4 wt%) and a Ni content of 4.4–6.1 wt%. Sulfides are troilite containing up to 0.78 wt% Ni. Representative analyses are given in Table 3.1

Table 4a. Electron microprobe (defocused beam) analyses of matrix within carbonaceous chondrites.

	Sahara									
	NWA 1152	00182	Renazzo ^a	Renazzo ^b	EET 877702	Al Rais ^a	Allende ^a	Allende ^b	Vigarano ^a	Vigarano ^b
Na ₂ O	0.13	0.27	1.16	0.78	0.54	0.98	0.22	0.05	0.49	0.59
SiO ₂	27.76	22.73	31.4	34.62	30.73	26.5	28.0	29.56	28.3	28.35
MgO	14.27	20.37	15.8	16.63	17.36	15.2	20.2	20.65	17.1	16.56
Al ₂ O ₃	4.15	1.11	2.66	3.07	2.02	2.13	2.30	1.69	4.27	4.33
SO ₃	1.90	5.87	7.96	5.99	8.22	7.45	2.82	1.12	0.51	0.40
K ₂ O	0.09	0.04	0.16	0.10	0.10	0.13	0.1	0.00	0.05	0.03
CaO	2.21	5.40	0.87	0.61	0.97	1.33	2.37	0.22	1.53	1.13
TiO ₂	0.06	0.18	0.7	0.06	0.08	0.6	0.9	0.09	0.9	0.07
Cr ₂ O ₃	0.37	0.75	0.35	0.31	0.44	0.32	0.38	0.49	0.40	0.44
MnO	0.23	0.13	0.33	0.23	0.26	0.17	0.21	0.20	0.14	0.25
FeO	36.51	30.74	24.3	27.47	33.10	22.2	31.9	36.86	32.6	41.47
NiO	1.82	1.60	1.48	2.14	1.78	2.15	1.83	0.63	1.39	3.40
Total	89.51	89.19	86.54	92.01	95.60	78.62	90.33	91.56	86.87	97.02

^aData from McSween and Richardson (1977).^bData from Zolensky et al. (1993). These analyses were obtained using a 3 μm focused electron beam; original data gives wt% S, values were converted to SO₃ for comparison with our data and McSween and Richardson (1977). McSween and Richardson (1977) and our data were obtained using broad, defocused beams (100 and 40 μm, respectively) for NWA 1152 and Sahara 00182. Low totals from defocused beam analyses are likely due to the presence of voids and surface roughness.

Table 4b. Si normalized elemental abundances (wt%) in carbonaceous chondrite matrix.

	Sahara											
	NWA 1152	00182	Renazzo ^a	Al Rais ^a	Mean CR ^a	Renazzo ^b	EET 877702	Allende ^a	Vigarano ^a	Mean CV ^a	Allende ^b	Vigarano ^b
Na/Si	0.007	0.018	0.059	0.059	0.59	0.036	0.028	0.012	0.028	0.20	0.003	0.033
Mg/Si	0.661	1.162	0.648	0.742	0.695	0.620	0.729	0.923	0.780	0.832	0.901	0.754
Al/Si	0.171	0.054	0.096	0.091	0.935	0.100	0.074	0.093	0.171	0.099	0.065	0.173
S/Si	0.060	0.249	0.218	0.241	0.261	0.148	0.229	0.086	0.015	0.068	0.032	0.012
K/Si	0.005	0.003	0.009	0.009	0.009	0.005	0.006	0.001	0.003	0.003	0.000	0.002
Ca/Si	0.119	0.399	0.042	0.077	0.060	0.027	0.048	0.129	0.083	0.105	0.011	0.061
Ti/Si	0.003	0.010	0.003	0.003	0.003	0.002	0.003	0.004	0.004	0.004	0.004	0.003
Cr/Si	0.020	0.049	0.016	0.018	0.017	0.013	0.021	0.020	0.021	0.020	0.024	0.023
Mn/Si	0.014	0.009	0.017	0.011	0.014	0.011	0.014	0.012	0.008	0.011	0.011	0.015
Fe/Si	2.223	2.448	1.289	1.396	1.343	1.319	1.791	1.892	1.916	1.838	2.074	2.433
Ni/Si	0.112	0.128	0.079	0.137	0.108	0.104	0.097	0.110	0.083	0.091	0.036	0.202

^aData from McSween and Richardson (1977) and references therein.^bData recalculated from Zolensky et al. (1993).

Refractory Inclusions

Refractory inclusions are rare in NWA 1152 (0.3 vol%) and are most commonly amoeboid olivine aggregates (AOAs) or spinel pyroxene aggregates (SPAs) (Fig. 4). The AOAs are generally larger than the SPAs (200–300 μm and 100–200 μm , respectively). All contain small nuggets of spinel ($\text{FeO} = \sim 0.9$ wt%) a few microns in size and are typically mantled by Al-rich diopside ($\text{Al}_2\text{O}_3 = 3.5$ –17.1 wt%). The spinel-pyroxene cores are surrounded by MgO-rich olivine with a composition of Fo_{97} . The SPAs are characterized by distinct cores of spinel ($\text{FeO} = \sim 1.4$ wt%) tens of microns in size, sometimes containing small blebs of perovskite, surrounded by rims or mantles of Ca-Al-Ti-rich diopside ($\text{Al}_2\text{O}_3 = 12.5$ –33.9, $\text{TiO}_2 = 1.1$ –6.1 wt%) and Al-rich diopside ($\text{Al}_2\text{O}_3 = 1.9$ –8.7 wt%). Some narrow (micron scale) rims of more ferroan olivine can be seen on the refractory inclusions (Fig. 4a), which suggests hydrothermal alteration on the asteroidal parent body (Krot et al. 1995 and references therein; Chizmadia et al. 2002). No melilite was observed in either inclusion type. Representative analyses are shown in Table 5.

Light Element Isotopic Composition

Two separate analyses of powdered and homogenized sample were carried out to determine the O isotope composition (sample weight = 1.991 and 1.907 mg). The mean compositions were $\delta^{17}\text{O} = -3.43 \pm 0.23\text{‰}$ (1σ); $\delta^{18}\text{O} = 0.70 \pm 0.44\text{‰}$ (1σ); $\Delta^{17}\text{O} = -3.77 \pm 0.03\text{‰}$ (1σ) (Fig. 5).

Carbon isotope analysis was carried out on two samples weighing 14.80 and 15.30 mg. The bulk carbon content

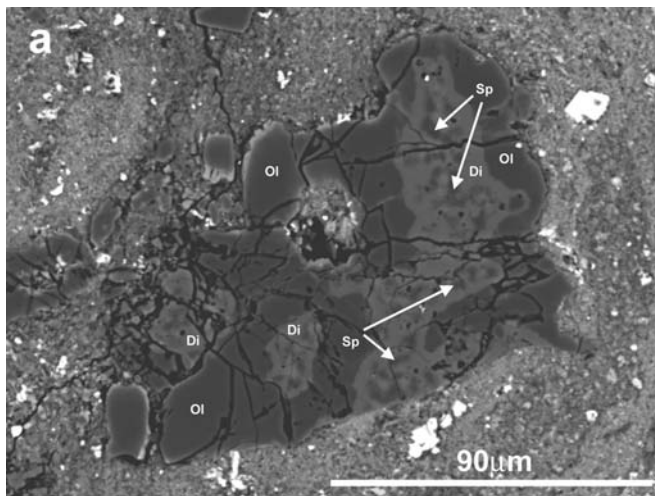


Fig. 4a. A BSE image of an amoeboid olivine aggregate in NWA 1152. The object has a core zone composed of spinel and diopside, which is almost completely surrounded by a rim of Mg-rich olivine. In some parts, the olivine mantle has a rim (few microns thick) of more ferroan olivine where it is contact with the matrix (notably the top center of the object).

measured was 1.1 wt% and mean $\delta^{13}\text{C}_{(\text{PDB})}$ composition was $-14.98 \pm 0.03\text{‰}$ (1σ).

Nitrogen analyses on a single sample weighing 1.878 mg indicated a bulk nitrogen content of 176.8 ng (96.3 ppm) with a $\delta^{15}\text{N}_{(\text{AIR})}$ composition of -16.7‰ .

Bulk elemental analyses were carried out using ICP-AES on two sub-samples of NWA 1152. Mg/Si ratios indicate that NWA 1152 is a carbonaceous chondrite; Al/Si ratios show similarities with the CR, CI, and CM chondrites and Ca/Si ratios show similarities with the CM, CO, CR, CI, and CH chondrites. Results are shown in Table 6.

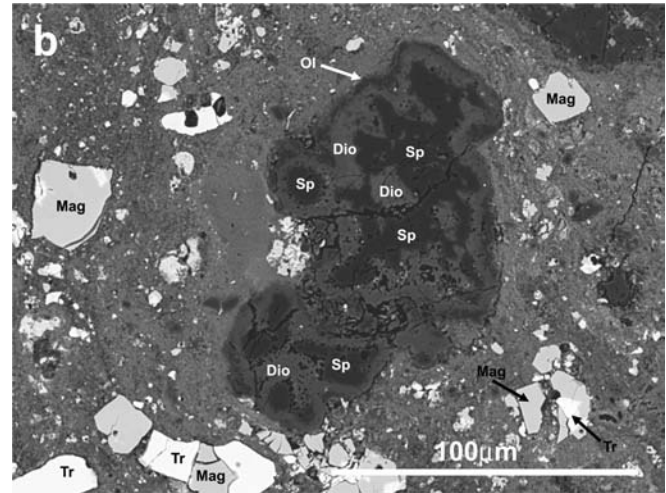


Fig. 4b. A BSE image of a spinel pyroxene aggregate in NWA 1152. This object is very similar in terms of mineralogy to the object shown in Fig. 4a. It is composed predominantly of a spinel core, which is entirely mantled in a rim of diopside a few microns thick. The diopside is itself rimmed with thinner mantle of olivine. Unlike the amoeboid olivine aggregate seen in Fig. 4a, no ferroan olivine is seen where the olivine rim is in contact with the matrix.

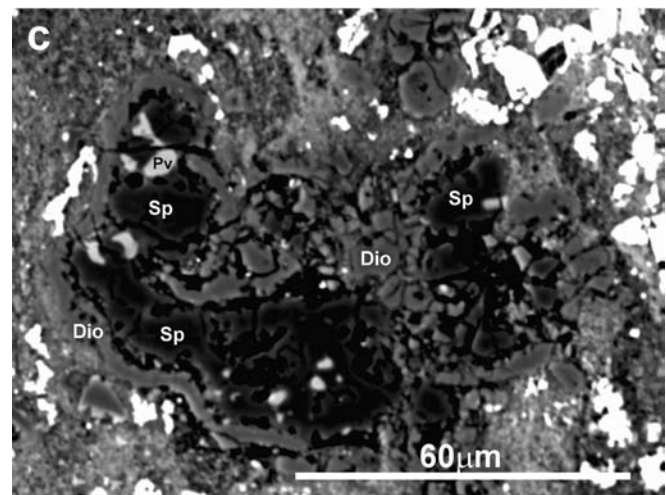


Fig. 4c. A BSE image of a spinel pyroxene aggregate in NWA 1152. This object is composed predominantly of spinel. Small (~ 3 μm) blebs of perovskite (light grey) can be seen in the spinel core. A rim of Ca-Al-Ti diopside surrounds the spinel and perovskite core.

Table 5. Representative analyses of phases in refractory inclusions within NWA 1152.^a

	Spinel		Pyroxene		Olivine	
Na ₂ O	bd	bd	bd	0.06	bd	bd
MgO	27.11	26.83	17.16	12.63	56.40	53.40
Al ₂ O ₃	70.93	71.01	4.70	12.46	bd	0.55
SiO ₂	0.11	0.22	52.10	44.13	42.32	41.16
CaO	0.09	0.47	25.03	25.36	0.25	0.08
TiO ₂	0.22	0.70	0.680	3.257	bd	bd
Ti ₂ O ₃	–	–	bd	1.479	–	–
Cr ₂ O ₃	0.17	0.12	0.11	0.05	0.16	0.15
MnO	bd	bd	bd	bd	bd	0.24
FeO	0.80	0.77	0.48	0.40	0.85	3.73
NiO	bd	bd	bd	0.07	bd	bd
Total	99.43	100.12	100.26	99.90	99.98	99.31
			Fs 0.76	Fs 0.71	Fo 99.2	Fo 96.2

^aP₂O₅, K₂O, and CoO were all below detection.

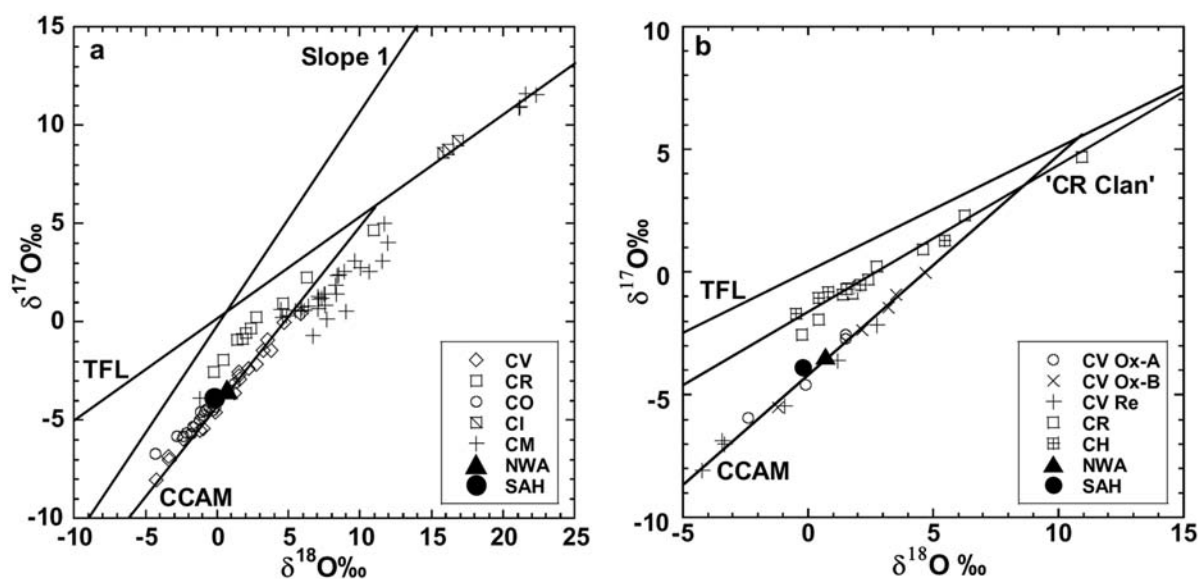


Fig. 5. a) Oxygen three-isotope graphs showing the composition of NWA 1152 and Sahara 00182 compared with the other carbonaceous chondrite groups, and b) compared with the CV and CR clan chondrites; TFL = terrestrial fractionation line, CCAM = carbonaceous chondrite anhydrous mixing line (Clayton et al. 1977), Slope 1 = slope 1.00 (Young and Russell 1998), “CR clan” line = slope 0.7 line defining CR and CR clan samples (Weisberg et al. 1995). Sahara 00182 data from Grossman and Zipfel (2001); carbonaceous chondrite data from Clayton and Mayeda (1999); NWA 1152 data from this study.

Description of Sahara 00182

Sahara 00182 is listed in *The Meteoritical Bulletin* (2001) as an ungrouped C3 meteorite and has been described as a possible CR3 chondrite (Weisberg 2001). A description of the mineralogy and petrography of Sahara 00182 is given here for comparison with NWA 1152. Figure 6 shows a Mg-Ca-Al X-ray mosaic of Sahara 00182.

Chondrules

Similar to NWA 1152, Sahara 00182 contains well-defined chondrules between approximately 200 μm and 3 mm in diameter, with the majority being type 1 PO chondrules,

with a few POP chondrules (Fig. 6). Often, the chondrules are fragmented or irregularly shaped; many contain large metal and sulfide blebs, heterogeneously distributed through the chondrule (Fig. 7a). Other chondrules contain blebs of Fe-Ni metal (with occasional sulfides), which are evenly distributed throughout (Fig. 7b), while some display a typical PO texture with rims of Fe-Ni metal blebs. Troilite (S mean = 35.7 wt%, range 35.0–36.6 wt%; Ni mean = 0.03 wt%, range 0–0.11 wt%) and Fe-Ni metal (Ni mean = 5.8 wt%, range 4.0–6.7 wt%) occur in the chondrules in approximately equal proportions, rare pyrrhotite is also observed. Some oxidation of the metal has occurred, although not to the degree as in NWA 1152. In the section available for study, one large multi-layered chondrule is rimmed with silica and is similar to

Table 6. Volatile-free bulk wet chemical analyses of NWA 1152 and Sahara 00182 and literature data from other chondrite groups.

Wt%	ALL Ref	ALL Ref ^a	NWA 1152	Sahara 00182	CR ^b	CV ^c	CI ^c	CM ^c	CO ^c	CK ^d	CH ^e	EH ^c	EL ^c	H ^c	L ^c	LL ^c
Si	29.1	28.5	27.9	28.4	27.4	27.9	18.8	23.1	28.4	27.0	23.8	29.9	33.2	30.2	33.1	33.8
Ti	0.1	0.2	0.1	0.1	0.2	0.2	0.1	0.1	0.1	0.2	0.1	0.1	0.1	0.1	0.1	0.1
Al	3.0	3.1	2.1	2.7	2.3	3.1	1.5	2.1	2.6	2.9	1.9	1.4	1.9	2.0	2.2	2.1
Cr	0.6	0.7	0.6	0.6	0.7	0.6	0.5	0.5	0.6	0.7	0.6	0.6	0.5	0.7	0.7	0.7
Fe	39.9	42.0	40.2	36.9	42.9	42.0	32.5	37.5	44.3	42.2	72.2	51.8	39.3	49.2	38.4	33.1
Mn	0.3	0.3	0.3	0.2	0.3	0.3	0.3	0.3	0.3	0.3	0.2	0.4	0.3	0.4	0.5	0.5
Mg	25.4	26.4	24.3	24.9	24.8	25.9	17.3	20.9	25.9	26.5	22.0	18.9	25.2	25.0	26.6	27.4
Ca	3.2	3.3	2.7	4.1	2.5	3.4	1.6	2.3	2.8	3.1	2.0	1.5	1.8	2.2	2.3	2.3
Na	0.5	0.6	0.1	0.3	0.6	0.6	0.9	0.7	0.7	0.6	0.3	1.2	1.0	1.1	1.3	1.3
K	0.1	0.1	0.1	0.0	0.1	0.1	0.1	0.1	0.1	0.1	0.0	0.1	0.1	0.1	0.1	0.1
P	0.2	0.2	0.2	0.2	0.2	0.2	0.2	0.2	0.2	0.1	–	0.4	0.2	0.2	0.2	0.2
Ni	2.3	2.3	1.4	1.9	2.4	2.4	1.9	2.1	2.5	2.3	4.4	3.1	5.9	2.9	2.1	1.8
Atomic ratios																
Mg/Si			1.008	1.012	1.045	1.066	1.066	1.042	1.053	1.127	1.063	0.731	0.871	0.954	0.925	0.928
Al/Si ($\times 10^4$)			787	992	865	1168	855	955	940	1109	828	505	585	693	684	655
Ca/Si ($\times 10^4$)			686	1018	631	853	615	692	695	799	598	358	380	520	497	482
Fe/Si			7254	6254	7875	7578	8719	8177	7847	7855	15222	8730	5934	8177	5838	4913
Ca/Al			0.872	1.026	0.73	0.73	0.72	0.72	0.74	0.72	0.72	0.71	0.65	0.75	0.73	0.74

^aThe values are normalized to 100%. Results from NWA 1152, Sahara 00182, and Allende reference material are means from two analyses of 50 mg sub-samples.

^bJarosewich et al. (1987).

^cData from Wasson and Kallemeyn (1988).

^dKallemeyn et al. (1991) except Si (Mason and Wiik 1962a).

^eWasson and Kallemeyn (1990) except Si (Scott 1988).

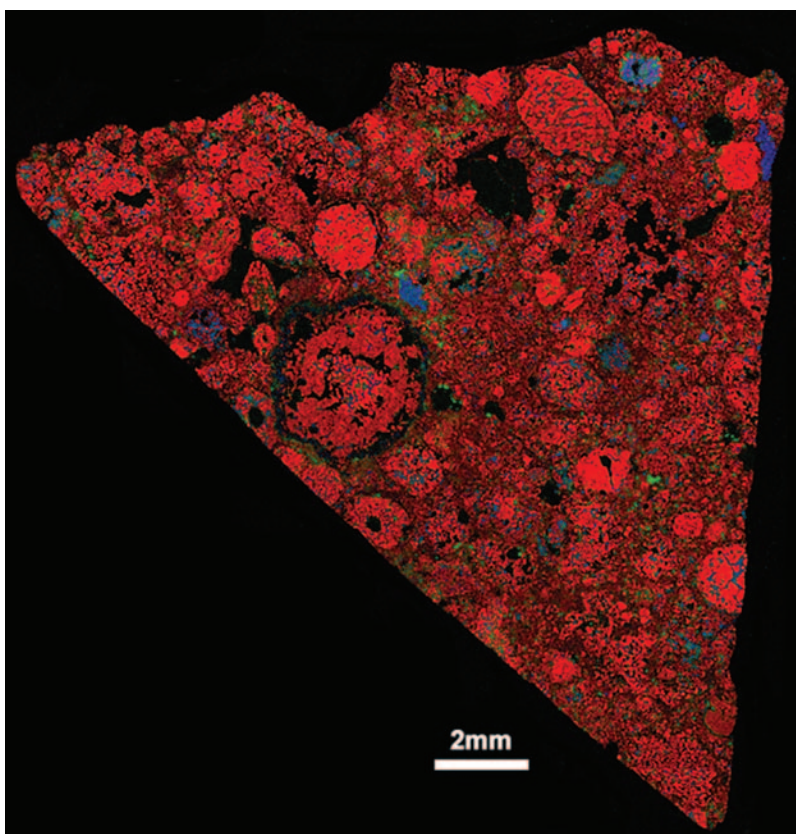


Fig. 6. X-ray elemental map of Sahara 00182 showing distribution of chondrules, matrix, and refractory inclusions; red = Mg, blue = Al, and green = Ca.

Table 7. Representative analyses of silicate and opaque phases within chondrules in Sahara 00182.^a

Silicates		Mesostasis					
		Chondrule grains		Diopside		Augite	
Olivine		Low-Ca Pyx	Diopside	Diopside	Augite	Diopside	Feldspar
Na ₂ O	bd	bd	0.07	0.19	0.16	0.08	2.67
MgO	50.35	35.36	16.02	27.72	19.88	15.20	0.05
Al ₂ O ₃	0.10	0.37	12.31	2.19	2.56	12.36	16.08
SiO ₂	41.16	57.77	46.31	54.34	52.53	46.62	12.53
K ₂ O	bd	bd	bd	bd	bd	bd	47.49
CaO	0.09	0.20	20.17	9.99	20.57	21.26	bd
TiO ₂	bd	0.12	1.23	0.71	1.01	0.94	21.05
Cr ₂ O ₃	0.08	0.08	2.57	0.51	0.48	2.51	1.07
MnO	0.22	0.16	0.25	0.21	0.13	0.31	1.30
FeO	7.83	7.61	0.83	4.15	1.90	0.73	0.29
CoO	bd	0.05	bd	bd	bd	bd	0.36
NiO	0.07	bd	bd	bd	bd	bd	bd
Total	99.9	100.03	99.76	100.01	99.22	100.01	100.32
	Fo 92.0	Fo 92.3	Fs 1.3	Fs 6.26	Fs 2.99	Fs 1.3	Fs 0.6
Metal and sulfides							
Chondrule grains		Rims		Fe-Ni Metal		Sulfide	
Fe-Ni Metal		Sulfide		Fe-Ni Metal		Sulfide	
Si	bd	bd	bd	bd	0.07	bd	bd
P	0.05	bd	bd	0.05	bd	bd	bd
S	bd	bd	36.09	bd	bd	35.49	35.75
Cr	bd	bd	0.07	0.05	bd	bd	0.08
Mn	bd	bd	bd	0.07	bd	bd	bd
Fe	92.76	94.02	63.82	93.40	94.11	63.31	63.60
Co	0.36	0.34	0.06	0.30	0.32	bd	0.08
Ni	6.22	5.65	bd	5.83	5.53	0.06	0.05
Total	99.39	100.01	100.04	99.7	100.03	98.86	99.56

^aPsO₅ was below detection in silicate phases. Ti was below detection limits in metal and sulfide phases.

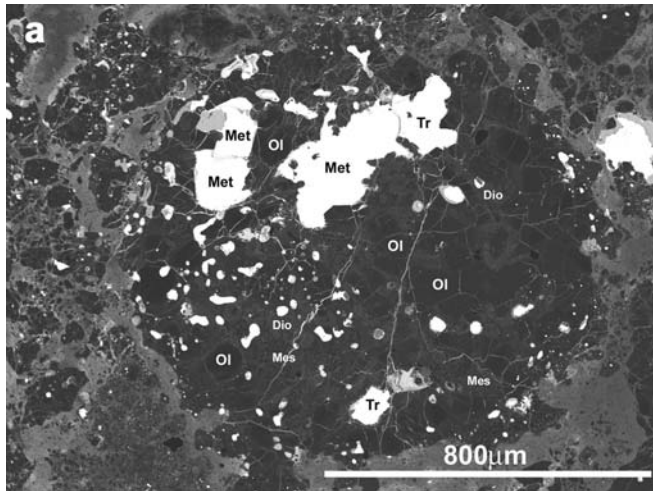


Fig. 7a. A BSE image of a metal and sulfide-rich chondrule in Sahara 00182. The chondrule has a porphyritic olivine-pyroxene morphology with grains of Mg-rich olivine and elongate grains of diopside. Mesostasis is crystalline and feldspathic in composition, with some micron sized grains crystallites of diopside. Toward the top of the chondrule are some large, irregularly shaped masses, a few hundred microns in size, of Fe-Ni metal and troilite. Some smaller Fe-Ni metal blebs can also be seen.

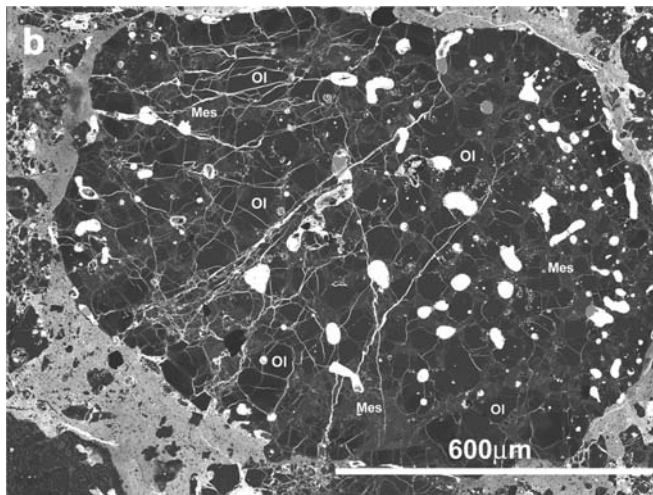


Fig. 7b. A BSE image of a metal-rich chondrule in Sahara 00182. This chondrule has a porphyritic olivine morphology and crystalline mesostasis with a feldspathic composition and diopside crystallites, as seen above. The Fe-Ni metal in this chondrule is more evenly distributed and occurs in rounded blebs, tens of microns in size. Prominent veins and veinlets of iron oxide crosscut the chondrule.

chondrules reported in Krot et al. (2002) (Fig. 7c). Olivine within the chondrules has a mean composition of $\text{Fo}_{92.2 \pm 0.64}$ (1σ) ($n = 129$, range 91.7–97.3) and occasionally the grains show some slight zonation, becoming more fayalitic toward the outside. Low-Ca pyroxene grains have a mean composition of $\text{Fs}_{4.4 \pm 1.8}$ (1σ) $\text{Wo}_{1.3 \pm 1.1}$ (1σ) and diopside grains a mean composition of $\text{Fs}_{1.6 \pm 0.2}$ (1σ) $\text{Wo}_{47.4 \pm 1.9}$ (1σ). Similar to chondrules in NWA 1152, veins of magnetite often

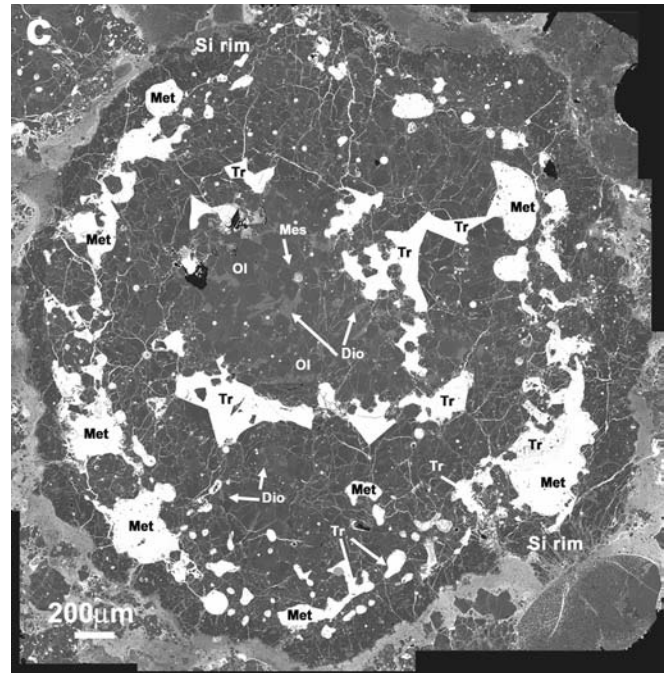


Fig. 7c. A BSE image of a multi-component chondrule in Sahara 00182. This object consists of a number of zones or portions, each having its own characteristics. The central portion displays a porphyritic olivine-pyroxene morphology, with glassy mesostasis. There are a few small blebs of Fe-Ni metal irregularly distributed in this central portion. Around the central portion are some large, angular masses, a few hundred microns in size, of troilite. Surrounding the troilite is a belt, between ~300 and 800 μm in width, of porphyritic olivine morphology. Mesostasis in this portion is crystalline and feldspathic in composition, with crystallites of diopside and is similar to that seen in chondrules above. Similar to the central portion, there are some small, micron sized blebs of Fe-Ni metal within the silicate phases. Around the porphyritic olivine belt are a number of rounded masses of Fe-Ni metal, with rare troilite, which are interconnected with narrow veins of iron oxide. The entire chondrule is rimmed with a mantle of silica, up to ~300 μm wide, with crystallites of Ca-feldspar.

crosscut the main body of the chondrules and also the rims. Chondrule mesostasis is mostly composed of feldspathic groundmass with high-Ca pyroxene and is crystalline, although the central portion of the Si-rimmed chondrule (Fig. 7c) has glassy mesostasis. Both augite (mean $\text{Fs}_{4.0 \pm 3.3}$ [1σ] $\text{Wo}_{38.1 \pm 6.4}$ [1σ]) and diopside (mean $\text{Fs}_{1.7 \pm 1.3}$ [1σ] $\text{Wo}_{48.8 \pm 3.9}$ [1σ]) contain Al_2O_3 (2.3–19.7 wt%); feldspathic mesostasis has a mean composition of $\text{Ab}_{18.5 \pm 5.3}$ (1σ) $\text{An}_{81.1 \pm 5.4}$ (1σ). Representative analyses of chondrule phases are shown in Table 7.

Matrix

Matrix within Sahara 00182 is composed of very fine-grained (sub-micron scale) silicates, which, being finer grained, lack the more granular appearance of those in NWA 1152 (Fig. 8). Similar to NWA 1152, phyllosilicates are not

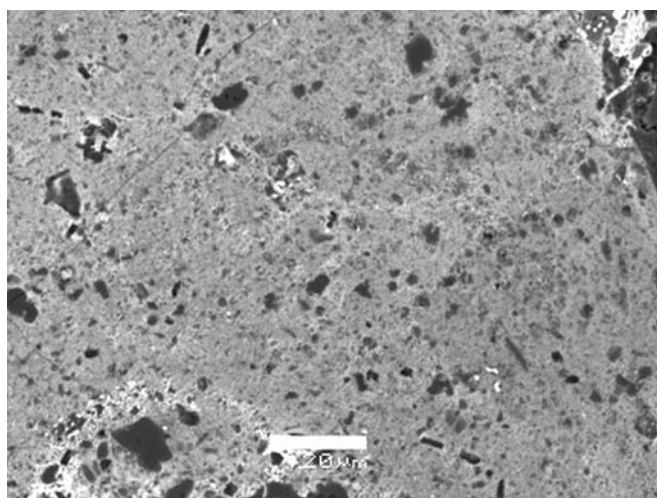


Fig. 8. A BSE image of representative matrix in Sahara 00182. The groundmass is composed of very fine grained, sub-micron silicates, which lack the granular appearance seen in NWA 1152. Within the matrix groundmass, larger more angular silicates occur, which are mostly Mg-rich olivine and range from ~10–20 μm in size. Smaller, rounded, micron sized grains of Mg-rich olivine can also be seen. Unlike matrix in NWA 1152, opaque phases are not often observed within matrix material.

observed within the matrix material. Some larger angular silicate grains are observed, which are usually 20–30 μm in size with some up to ~50 μm . These silicate grains are composed of olivine (mean $\text{Fo}_{91.9 \pm 0.4}$) or low-Ca pyroxene (mean $\text{Fs}_{6.7 \pm 2.5}$ [1 σ] $\text{Wo}_{1.3 \pm 0.7}$ [1 σ]) in approximately equal proportions, rare augite and plagioclase grains are also observed. Bulk analyses of matrix have been determined by electron microprobe analyses using a defocused beam (40 μm diameter), results are shown in Table 4a and Si normalized values in Table 4b. Representative analyses of larger grains are also given in Table 8.

Isolated Opaques

Unlike NWA 1152, small Fe-Ni metal and sulfide grains are not observed within the matrix, instead there are a number of prominent rounded or irregularly shaped masses of Fe-Ni metal and sulfide. The irregularly shaped masses are up to about 1.8 mm in size and are composed of both Fe-Ni metal (Ni mean = 5.8 wt%, range 5.5–6.2 wt%) and troilite (S mean = 35.7 wt%, range 35.5–35.8 wt%). The rounded masses are smaller (approximately 500 μm in diameter) and are composed only of Fe-Ni metal (Ni mean = 5.7 wt%, range

Table 8. Analyses of silicate and isolated opaque phases within matrix in Sahara 00182.^a

	Silicate Grains			Pyroxene					
	Olivine								
Na ₂ O	0.09	bd	bd	0.08	bd	bd			
MgO	50.70	50.60	51.10	25.56	35.27	37.77			
Al ₂ O ₃	0.21	0.12	bd	1.95	0.73	0.63			
SiO ₂	41.08	41.55	40.69	53.52	56.57	58.36			
CaO	0.07	0.07	0.06	8.22	0.71	0.41			
TiO ₂	0.09	bd	bd	0.84	0.14	0.08			
Cr ₂ O ₃	0.12	0.22	bd	0.95	0.34	0.33			
MnO	0.14	0.24	0.21	0.33	0.19	0.09			
FeO	7.88	7.51	8.15	8.96	6.38	2.99			
CoO	bd	bd	0.05	bd	bd	bd			
NiO	0.08	bd	bd	bd	0.12	bd			
Total	100.46	100.31	100.26	100.41	100.45	100.66			
	Fo 92.0	Fo 92.3	Fo 91.8	Fs 13.8	Fs 9.1	Fs 4.2			
	Isolated Opaque phases			Irregularly shaped grains			Sulfides		
	Small rounded grains			Fe-Ni metal					
Si	bd	0.14	bd	bd	bd	0.05	bd	bd	bd
P	bd	bd	bd	0.05	bd	bd	bd	bd	bd
S	bd	bd	bd	bd	bd	bd	35.48	35.76	35.82
Cr	bd	bd	bd	0.05	bd	bd	0.09	0.07	0.07
Mn	bd	0.05	bd	bd	bd	bd	bd	bd	bd
Fe	93.53	93.41	93.87	93.86	93.55	93.83	63.66	63.10	63.42
Co	0.27	0.32	0.34	0.29	0.35	0.34	bd	0.06	bd
Ni	5.72	5.83	5.94	5.67	5.84	5.70	bd	0.08	0.05
Total	99.52	99.75	100.15	99.92	99.74	99.92	99.23	99.07	99.36

^aP₂O₅ and K₂O were below detection limits in silicate phases. Ti was below detection in metal and sulfide phases.

5.3–5.9 wt%). Similar to chondrule metal, some of the matrix metal has been oxidized. Analyses of opaque phases within matrix are given in Table 8.

Refractory Inclusions

Like NWA 1152, refractory inclusions are not abundant and comprise just 1.1 vol% of the section studied. One prominent inclusion is a fine-grained spinel-rich “fluffy” CAI (Fig. 9a), composed of many layered nodules (Fig. 9b) up to approximately 50 μm in size with cores of Cr_2O_3 and FeO-rich

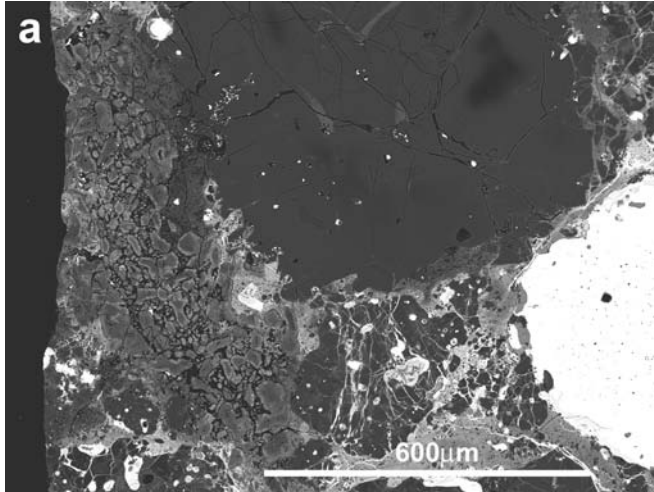


Fig. 9a. A BSE image of the “fluffy” spinel-rich refractory inclusion in Sahara 00182. The object is at the left hand side of the image and the individual spinel nuggets can clearly be seen. At the top of the image is part of a porphyritic olivine chondrule, note the zonation in the olivine.

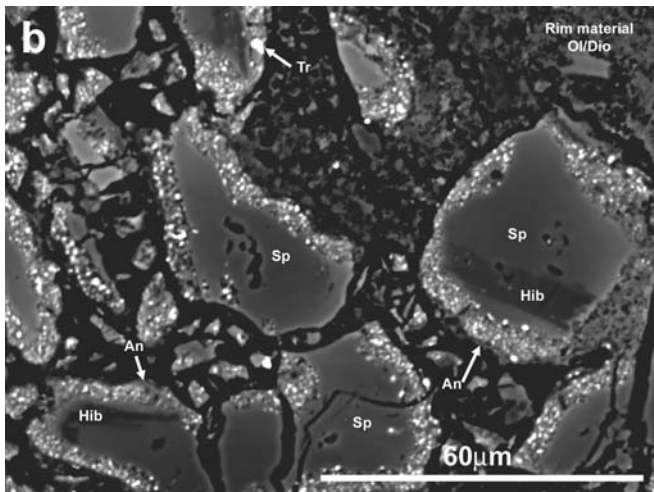


Fig. 9b. A high-magnification, BSE image of spinel nuggets from the “fluffy” refractory inclusion. The individual nuggets are up to $\sim 50 \mu\text{m}$ in size and composed primarily of spinel, with occasional laths of hibanite. The nuggets are rimmed with a layer of anorthite with abundant blebs of Fe-Ni-S. The whole object is rimmed with fine-grained olivine and pyroxene.

spinel (mean $\text{Cr}_2\text{O}_3 = 11.4 \text{ wt\%}$, range 7.3–15.0 wt%; $\text{FeO} < 9.9 \text{ wt\%}$), some of which contain hibanite laths. The spinel \pm hibanite cores are surrounded by a layer (up to 5 μm wide) of anorthite with abundant small, sub-micron-sized blebs of Fe-Ni-S-O, which is itself followed by a layer of anorthite (Fe-Ni-S-O free) and then, occasionally, a layer of Ca-rich pyroxene. One other large ($\sim 800 \mu\text{m}$ across) refractory inclusion is observed within the section (Figs. 10a and 10b) and is an Al-rich chondrule. This compact inclusion has a rounded shape and is composed primarily of Al-Ti-rich diopside (mean $\text{Al}_2\text{O}_3 = 14.1 \text{ wt\%}$, range 11.0–16.4 wt%; mean $\text{TiO}_2 = 2.2 \text{ wt\%}$, range 0.5–3.8 wt%). In addition to the dominant pyroxene phase, spinel grains ($\text{Cr}_2\text{O}_3 < 1.3 \text{ wt\%}$, $\text{FeO} < 6.7 \text{ wt\%}$) up to approximately 20 μm wide, occur toward the center of the object. Further toward the rim, elongate laths of

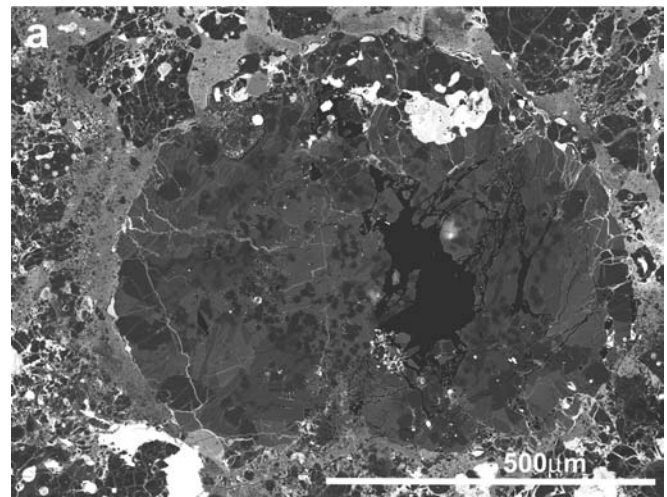


Fig. 10a. A BSE image of the Al-rich chondrule in Sahara 00182.

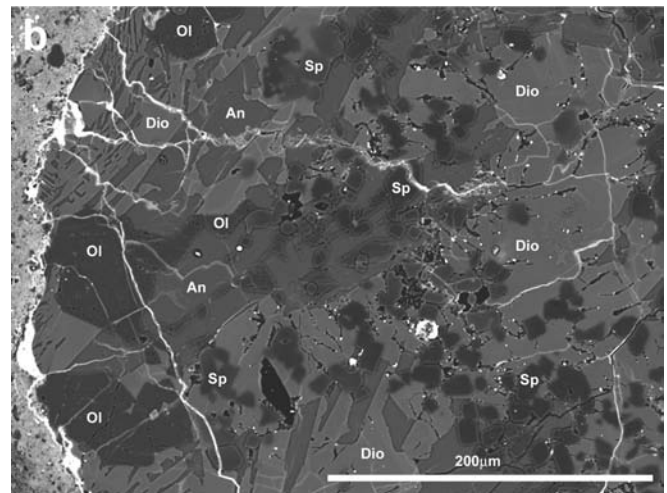


Fig. 10b. A high-magnification, BSE image of a region of the Al-rich chondrule in Sahara 00182. The majority of the chondrule is composed of Al-Ti diopside with anorthite. Spinel grains, up to $\sim 20 \mu\text{m}$ in size, occur throughout the object except in the $\sim 75 \mu\text{m}$ toward the rims, where Mg-rich olivine grains occur.

plagioclase ($\text{Ab}_{5.2 \pm 0.7 [1\sigma]} \text{An}_{94.7 \pm 0.7 [1\sigma]} \text{Or}_{0.2 \pm 0.1 [1\sigma]}$) can be seen along with Al-Ti-rich diopside (mean $\text{Al}_2\text{O}_3 = 13.2$ wt%, range 9.7–17.9 wt%; mean $\text{TiO}_2 = 3.7$ wt%, range 2.1–6.3 wt%) and olivine grains (Fo_{92}). Two objects are also observed, which appear to be fragments of mesostasis from larger Al-rich chondrules (Fig. 11). These are composed of glassy, feldspathic mesostasis ($\text{Na}_2\text{O} = 3.3$ – 4.3 wt%; $\text{Al}_2\text{O}_3 = 27.7$ – 30.9 wt%; $\text{CaO} = 8.9$ – 9.9 wt%) with angular grains of augite ($\text{TiO}_2 = 0.7$ – 1.1 wt%) and low-Ca pyroxene. Analyses of phases within refractory inclusions are shown in Table 9.

Light Element Isotopic Composition

The oxygen isotopic composition of Sahara 00182 was measured by R. N. Clayton and T. K. Mayeda at the University of Chicago. The values are reported in *The Meteoritical Bulletin* (2001); $\delta^{17}\text{O} = -3.89\%$, $\delta^{18}\text{O} = -0.19\%$ (Grossman and Zipfel 2001) (Fig. 5).

Carbon isotope analysis was carried out on a single sample weighing 26.668 mg. The bulk carbon content measured was 0.16 wt% with a $\delta^{13}\text{C}_{\text{(PDB)}}$ composition of -16.06% .

Table 9. Representative analyses of phases within the compact refractory inclusion/Al-rich chondrule and “fluffy” inclusion in Sahara 00182.^a

	Compact inclusion/Al-rich chondrule						Fluffy inclusion Nodule core					
	Diopside Center		Edge	Spinel		Plagioclase		Olivine	Spinel			
Na ₂ O	bd	bd	bd	0.07	0.05	0.06	0.53	0.72	bd	bd	0.22	
MgO	14.24	14.62	12.46	12.47	67.15	66.69	0.10	0.10	51.12	20.33	19.19	
Al ₂ O ₃	12.06	11.02	13.28	14.29	22.36	22.23	35.14	34.88	0.127	58.19	56.87	
SiO ₂	46.75	46.82	43.24	43.72	0.06	0.05	43.63	44.35	41.24	0.11	3.13	
P ₂ O ₅	bd	bd	bd	0.06	bd	bd	bd	bd	bd	bd	bd	
CaO	24.78	24.60	24.28	24.83	0.12	0.18	19.63	19.36	0.09	0.09	0.97	
TiO ₂	1.83	2.21	2.21	2.65	0.09	0.15	0.05	0.07	0.17	bd	bd	
Ti ₂ O ₃	0.118	0.123	3.719	0.90	–	–	–	–	–	–	–	
Cr ₂ O ₃	0.20	0.23	0.12	0.19	0.52	1.07	bd	bd	bd	10.20	8.80	
MnO	bd	bd	bd	0.05	0.08	0.08	bd	bd	0.25	0.13	0.12	
FeO	0.16	0.23	0.17	0.24	6.30	6.42	0.09	0.07	7.71	8.53	8.17	
Total	100.14	99.85	99.48	99.47	96.73	96.93	99.17	99.55	100.71	97.58	97.25	
	Fs 0.3	Fs 0.4	Fs 0.3	Fs 0.4	–	–	An 95.2	An 93.6	Fo 92.2	–	–	

^aK₂O, CoO, and NiO were below detection limits.

Table 10. Summary of mineralogy, petrography, light element isotope composition and bulk chemical compositions of NWA 1152 and Sahara 00182.

	NWA 1152	Sahara 00182	CRs	CVs	
Petrography ^a	Chondrule abundance (vol%)	52.2	64.9	37.0–63.1	33.0–52.5
	Chondrule diameter (mean, mm)	0.90	1.01	0.7	1.0
	Opaque phases (vol%)	4.1	6.9	4.8–10.2	3.1–4.8
	Matrix (vol%)	42.8	27.6	29.7–63.0	34.5–51.3
	Refractory inclusions	–	–	–	–
	(vol%)	0.3	1.1	0.1–2.6	6.1–11.5
	Matrix/chondrule ratio	0.82	0.43	0.60–1.85	0.55–1.17
Mean mineral composition (chondrule phases) ^b	Olivine (Fo)	98.8	92.2	97–99	92–96
	Low-Ca pyroxene	Fs 2.3 Wo 1.2	Fs 4.4 Wo 1.3	Fs 2–20 Wo 0.6–1.0	Fs 1–25 Wo 1–50
	Light element isotopes	$\delta^{13}\text{C}$ (‰) ^c	–15.0	–16.1	–6.0 to +12.1
	$\delta^{15}\text{N}$ (‰) ^d	–16.7	–14.1	~+100 to +190	~–9 to –45
	$\Delta^{17}\text{O}$ (‰) ^e	–3.77	–3.99	–2.42 to –0.96	–5.87 to –2.48
Bulk composition ^f	Mg/Si	1.008	1.012	1.045	1.066
	Al/Si ($\times 10^4$)	787	992	865	1168
	Ca/Si ($\times 10^4$)	686	1018	631	853

^aSee Table 1 for references.

^bCV compositions (Brearley and Jones 1998 and references therein); CR compositions (Bischoff et al. 1993; Weisberg et al. 1993; Kallemeyn et al. 1994).

^cCRs (Ash and Pillinger 1995); CVs (Kerridge 1985 and references therein; Pearson 2003).

^dCRs (Ash and Pillinger 1995; Weisberg et al. 1995 and references therein; Pearson 2003); CVs (Kerridge 1985; Pearson 2003).

^eSahara 00182 O isotope data (Grossman and Zipfel 2001); CV and CR data (Clayton and Mayeda 1999).

^fSee Table 6 for references.

Nitrogen analyses on a single sample weighing 0.737 mg indicated a bulk nitrogen content of 22.53 ng (30.6 ppm) with a $\delta^{15}\text{N}_{(\text{AIR})}$ composition of -14.1% .

Bulk elemental analyses were carried out using ICP-AES on two sub-samples of Sahara 00182. Similar to NWA 1152, Mg/Si ratios show that Sahara 00182 is a carbonaceous chondrite. Al/Si ratios are most similar to CM and CO chondrites but Ca/Si ratios are higher than literature values for other chondrite groups. This is most likely owing to the high degree of terrestrial weathering seen in Sahara 00182. Results are shown in Table 6.

DISCUSSION

Classification

Both NWA 1152 and Sahara 00182 have characteristics similar to the CV and CRs, however, neither meteorite can be easily assigned to either the CV or CR groups. This is shown by the different mineralogical, petrographic, and compositional characteristics, compared with those previously given for the CV and CR chondrites.

Petrography and Modal Abundances

Table 1 shows the modal analyses of phases within NWA 1152 and Sahara 00182 and data for CV and CR samples. The abundance of chondrules and chondrule fragments in NWA 1152 falls into the range defined by both the CRs and the CVs, although it is at the maximum end of the range for CV chondrites. Sahara 00182 on the other hand has a far greater abundance of chondrules and fragments than reported abundances for CV chondrites and, indeed, exceeds the maximum value reported for CRs.

Opaque phases within NWA 1152 fall into the range as

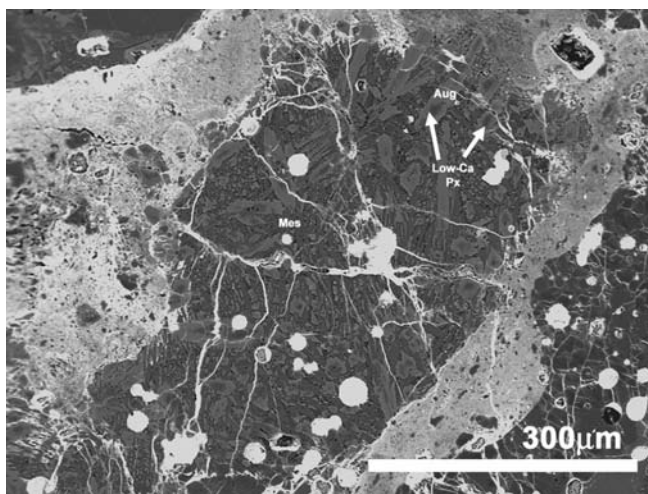


Fig. 11. A BSE image of a fragment of Al-rich chondrule mesostasis in Sahara 00182. The object is composed of glassy feldspathic mesostasis, with grains of low-Ca pyroxene and augite. Rounded blebs of Fe-Ni metal are also distributed throughout the object.

defined by the CVs and are slightly less abundant than reported for CRs. The abundance of opaque phases within Sahara 00182 falls into the reported range for CRs.

Matrix abundance in NWA 1152 is in the range reported for both CVs and CRs. For Sahara 00182, the matrix abundance is lower than for CVs or CRs.

Unlike typical CV samples, refractory inclusions in both NWA 1152 and Sahara 00182 are rarely observed. This low abundance in refractory inclusions is more typical of CR chondrites and the modal abundances measured for both samples fall into the range reported for CR samples.

Figure 12 shows the size frequency distributions of chondrules within NWA 1152 and Sahara 00182. The mean

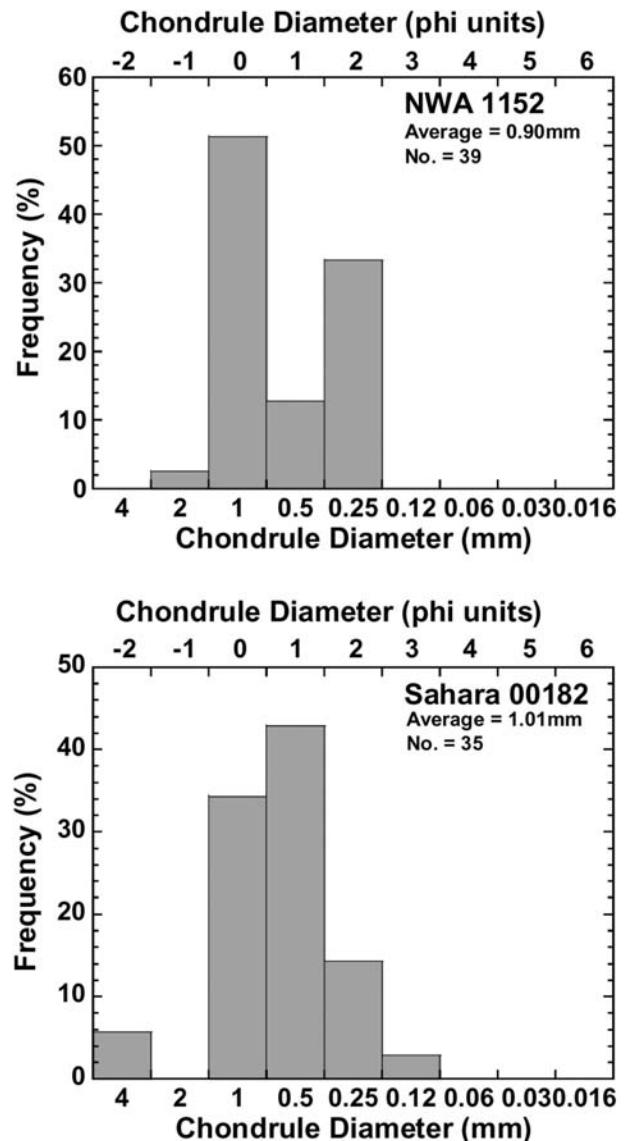


Fig. 12. Size distribution of chondrules in NWA 1152 and Sahara 00182. Chondrules in NWA 1152 have an average apparent diameter of 0.90 mm and Sahara 00182 chondrules 1.01 mm. Apparent chondrule diameters are more similar to CV chondrites than CR chondrites. Φ units = $-\log_2 d$, where d = apparent chondrule diameter in millimeters.

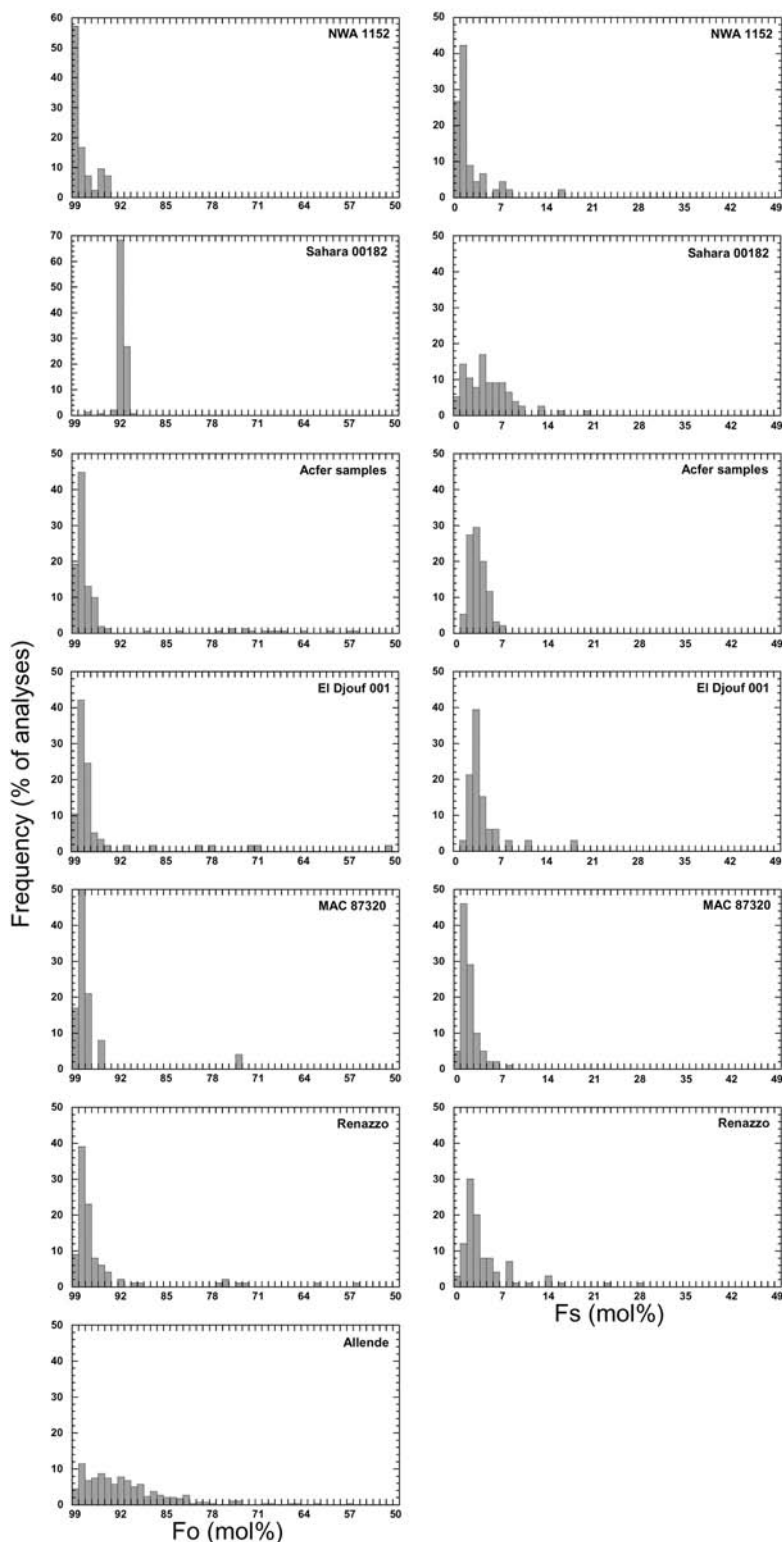


Fig. 13. Histograms showing olivine (left) and pyroxene (right) compositions in chondrules from NWA 1152 and Sahara 00182, with data from MAC 87320, Renazzo (Kallemeyn et al. 1994), Acfer samples, El Djouf 001 (Bischoff et al. 1993) and Allende (Simon et al. 1995) for comparison. Olivine compositions in NWA 1152 are extremely MgO-rich and similar to other CR chondrite samples. Olivine in Sahara 00182 is less MgO-rich than NWA 1152 or the CR chondrites, although does not show the range in composition as seen in Allende. Pyroxene in NWA 1152 shows the restricted range of composition as displayed by other CR chondrites. Sahara 00182 shows a broader range of composition, although is similar to Renazzo.

chondrule diameter of both samples (0.90 mm, NWA 1152; 1.01 mm, Sahara 00182) is larger than for CR chondrites (average ~0.7 mm) and are similar to values given for CV chondrites (~1 mm) (Grossman et al. 1988; Rubin 2000).

Mineral Compositions

Figure 13 shows histograms of olivine and pyroxene compositions measured in NWA 1152 and Sahara 00182 compared to olivine and pyroxene in CR chondrites from the Acfer region (059, 087, 097, 114, 139, 186, 187, 207, and 270) and El Djouf 001 (Bischoff et al. 1993), MAC 87320, Renazzo (Kallemeyn et al. 1994) and Allende (CV) (Simon et al. 1995). NWA 1152 has extremely MgO-rich olivine compositions and a very narrow range of olivine compositions, both of which are characteristic of CR chondrites. Sahara 00182 olivine compositions also show a narrow range although are slightly less enriched in MgO compared with NWA 1152 and the other CR chondrites. Some chondrule olivines show slight zonation, although this is relatively rare (Fig. 9a). The composition of Sahara 00182 olivine is similar to that seen in Allende, although Allende and indeed other CV chondrites display a far greater range of olivine compositions compared with the CRs.

Pyroxene grains in NWA 1152 and Sahara 00182 also display MgO enrichment and Fig. 13 also shows histograms of pyroxene compositions in the two samples compared with other CR samples. Similar to pyroxene in CR chondrites, pyroxene within NWA 1152 shows the restricted compositional range with the dominant compositions between Fs_1 and Fs_5 (Bischoff et al. 1993; Kallemeyn et al. 1994). Sahara 00182, however, shows a broader range in compositions with the peak between Fs_2 and Fs_8 and is more similar to pyroxene seen in Renazzo (Bischoff et al. 1993) than the desert samples from Acfer, El Djouf 001, or MAC 87320 (Bischoff et al. 1993; Kallemeyn et al. 1994).

Mesostasis in NWA 1152 is feldspathic in composition and usually crystalline, often containing crystallites of high- and low-Ca pyroxene, although some glassy mesostasis can be seen. Similarly mesostasis in Sahara 00182 is usually crystalline, although in some chondrules (notably the Si-rimmed multi-component chondrule, Fig. 7c) glassy mesostasis remains. Mesostasis in CR chondrite chondrules can range from that which is completely altered to chlorite- or serpentine-rich phyllosilicates, to that which is unaltered and fresh. Weisberg et al. (1993) note that chondrules with unaltered mesostases can be observed micrometers from chondrules with hydrated, phyllosilicate-rich mesostases, in the same thin section. In the Acfer/El Djouf 001 samples all the chondrules investigated have relatively unaltered, feldspathic mesostasis, which may be glassy, re-crystallized or fine-grained (Bischoff et al. 1993; Weisberg et al. 1993). Mesostases in CV chondrite chondrules are predominantly holocrystalline comprising plagioclase and Ca-rich pyroxene;

glassy mesostasis is rarely observed (Ikeda and Kimura 1995; Brearley and Jones 1998). Metasomatic reactions have altered the mesostasis in many CV chondrite chondrules, where amorphous or partly crystalline mesostasis is replaced by nepheline, sodalite, and minor amounts of grossular, wollastonite, andradite, kirschsteinite, and hedenbergite (Murakami and Ikeda 1994; Ikeda and Kimura 1995; Kimura and Ikeda 1995). The fact that glassy mesostasis is found in chondrules from both NWA 1152 and Sahara 00182, and the absence of phases such as sodalite and nepheline produced through metasomatism, indicates that their chondrules are relatively primitive. Similarly, the lack of phyllosilicates suggests that they have not suffered extensive aqueous alteration on the parent body. The chondrule mesostases in NWA 1152 and Sahara 00182 are most similar to that described for the Acfer/El Djouf 001 CR chondrite samples (Bischoff et al. 1993; Weisberg et al. 1993).

Refractory inclusions in NWA 1152 and Sahara 00182, in addition to being rarely observed, are unusual compared with inclusions typically found in CV or CR chondrites owing to the fact that no melilite is observed in any of the inclusions (MacPherson et al. 1988; Kallemeyn et al. 1994; Brearley and Jones 1998; Krot et al. 2002). Spinel pyroxene aggregates and amoeboid olivine aggregates seen in NWA 1152 are similar to those described in CR chondrites (Kallemeyn et al. 1994; Weber and Bischoff 1997; Krot et al. 2002) with the exception that melilite is not observed. In this respect, they are perhaps more similar to objects in Cold Bokkeveld (CM2) described by Greenwood et al. (1994) (see Figs. 4a and 4b of Greenwood et al. 1994) and the melilite-free inclusions in MAC 87300 and MAC 88107 (Russell et al. 2000). No melilite-rich inclusions can be found although, along with the SPAs and AOAs, melilite-rich inclusions are the dominant types of refractory inclusion found within CR chondrites (Weber and Bischoff 1997; Krot et al. 2002). The absence of melilite is likely to be as a result of secondary alteration of primary CAI components (Greenwood et al. 1994; Lee and Greenwood 1994; Krot et al. 1995). Melilite is the most readily affected primary CAI phase and will alter to anorthite, diopside, andradite, hedenbergite, grossular, and monticellite-kirschsteinite during metasomatism. The Fe-Ni-S-O phase seen as rims around spinel nuggets in the “fluffy” CAI is similar to the tochilinite phase in CM chondrites described by Tomeoka et al. (1998), which has been suggested as forming through reactions between kamacite and sulfur-bearing fluids. The presence of Cr_2O_3 and FeO within spinel in Sahara 00182 refractory inclusions also indicates a history of thermal metamorphism, which is consistent with the lack of observed phyllosilicates (Krot et al. 1995). The presence of ferroan olivine rims on some of the SPAs in NWA 1152 also signals aqueous and thermal alteration events occurring on the parent body (Krot et al. 1995, 1997; Chizmadia et al. 2002).

The majority of matrix metal grains in NWA 1152 have high Ni contents, typically around 50 wt%. Metal with high

Ni content has previously been reported from CV chondrites (Fuchs and Olsen 1973; McSween 1977; Krot et al. 1995), and has been suggested as forming through the oxidation of primary metal and redistribution of nickel during low-temperature aqueous alteration on the asteroidal parent body (Krot et al. 1995). The presence of abundant sulfides in Sahara 00182, occurring in both chondrules and matrix is highly unusual for CR chondrites. Sulfides commonly occur in CV chondrites, although not to the same extent as seen in Sahara 00182. Similar to the formation of high-Ni metal, sulfides in CVs have been suggested to form by the redistribution of sulfur during parent body metamorphism (Krot et al. 1995).

Previous studies have found that Fe-Ni metal in chondrules from CR chondrites display a positive Ni-Co trend and overlap with the CI abundance ratio (Anders and Grevesse 1989; Weisberg et al. 1993; Connolly et al. 2001; Krot et al. 2002). Figure 14 shows Ni content versus Co content plotted for Fe-Ni metals in NWA 1152 and Sahara 00182 chondrules compared with values for CR and CV chondrites (Fuchs and Olsen 1973; Connolly et al. 2001). Although some of the data overlap with the CI ratio, the majority of the data fall on the high Co side of the line. Metal from Sahara 00182 chondrules is more similar to that seen in CR samples (Connolly et al. 2001), although high-Ni content metal (~8–14 wt%) is not found. NWA 1152 metal shows similarity in Co content with CR samples, although has slightly lower Ni contents (Connolly et al. 2001). Neither NWA 1152 or Sahara 00182 have Co contents similar to the CVs (Fuchs and Olsen 1973). Also the positive Ni-Co trend described for CR chondrite chondrules is not well displayed by these samples. This disruption of positive Ni-Co correlation may be due to redistribution of nickel and/or cobalt during parent body alteration.

Matrix in NWA 1152 and Sahara 00182 is predominantly fine-grained (micron to sub-micron in size), with matrix in NWA 1152 being slightly coarser than matrix seen in Sahara 00182 (see Figs. 3 and 8). Unlike the CR chondrites, phyllosilicates are not observed in either NWA 1152 or Sahara 00182. Similarly, the abundant Ca-Fe pyroxenes and lath-shaped, ferrous olivines characteristic of CV chondrite matrix are not seen (Krot et al. 1995, 1997, 1998). Matrix compositions have been determined by broad (defocused) electron microprobe analyses and are shown in Table 4a. Comparing elemental abundances, normalized with respect to Si, of CR and CV chondrites shows that the abundances of Al, K, Ti, Cr, Mn, and Ni are quite similar in both groups (Table 4b). Na/Si ratios in NWA 1152 and Sahara 00182 matrix are low and similar to CV chondrites. Mg/Si abundance in NWA 1152 is similar to values reported for CRs, whereas Sahara 00182 shows a higher Mg/Si ratio in matrix than CV or CR chondrites (McSween and Richardson 1977). Sulfur in carbonaceous chondrite matrix shows a well-defined trend, where S/Si ratios decrease with

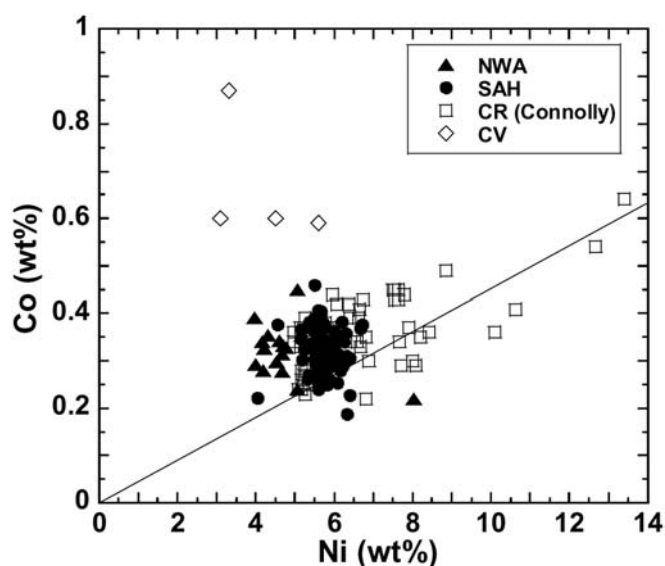


Fig. 14. Plot of Ni versus Co for chondrule metal in NWA 1152, Sahara 00182, CR, and CV chondrites. The solid line shown is the CI abundance Ni:Co ratio (Anders and Grevesse 1989); Fe-Ni metal from CR chondrites falls along, and overlaps, this line (see Fig 4; Weisberg et al. 1992). CV data from Fuchs and Olsen (1973), CR data from Connolly et al. (2001).

increasing petrologic type ($C1 > C2 > C3$) (McSween and Richardson 1977). S/Si abundance in NWA 1152 matrix is low and similar to CV values, while in Sahara 00182 S abundance is much higher and similar to CR values. Like sulfur, calcium in carbonaceous chondrite matrix also shows trend in abundance according to petrologic type, with Ca/Si abundance increasing slightly in the order $C3 > C2 > C1$, although there is quite a high degree of variability within each group (McSween and Richardson 1977). Ca/Si ratios in both NWA 1152 and Sahara 00182 matrix have similar abundances (or slightly higher) than CV chondrites, although both samples contain CaCO_3 weathering products, thus Ca abundance is likely to be erroneously high. Fe/Si ratios in NWA 1152 and Sahara 00182 are higher than values for CR and CV chondrites. McSween and Richardson (1977) report no clear difference in matrix Fe/Si ratios between CR and CV chondrite samples. Ni/Si ratios in carbonaceous chondrite matrix are similar in C1 and C3 samples, with C2 samples showing higher Ni/Si ratios. Ni/Si ratios in NWA 1152 and Sahara 00182 both show similarities with CR chondrites.

Light Element Isotope Composition

The oxygen isotopic compositions of both NWA 1152 and Sahara 00182 fall into the field defined by CV chondrites on an oxygen three-isotope plot (Fig. 5). The compositions are similar in terms of $\delta^{18}\text{O}$, although are ^{17}O depleted by approximately 1.5‰ compared with CR chondrites.

Carbon in Antarctic CR chondrites ranges from 1.2 to

3.4 wt%, with a range in $\delta^{13}\text{C}_{(\text{PDB})}$ of -5.0 to 13.3% ; Acfer desert samples 0.3 to 0.6 wt%, $\delta^{13}\text{C}_{(\text{PDB})}$ -6.0 to 12.1% and CR falls 1.3 to 2.7 wt%, $\delta^{13}\text{C}_{(\text{PDB})}$ -5.3 to -12.2% (Grady et al. 1991; Ash and Pillinger 1995; Bischoff et al. 1993; Pearson, 2003). Carbon abundance in CV chondrites ranges between 0.3 and 1.8 wt%, mean 0.77 wt% with $\delta^{13}\text{C}_{(\text{PDB})}$ -12.8 to -23.7% , mean -18.1% (Kerridge 1985 and references therein; Pearson 2003). Results from NWA 1152 are 1.1 wt%, with a $\delta^{13}\text{C}_{(\text{PDB})}$ of -15.0% , which is in the carbon abundance range for both CRs and CVs but is isotopically more similar to CV carbon. Sahara 00182 only contains 0.16 wt% carbon, with a $\delta^{13}\text{C}_{(\text{PDB})}$ of -16.1% , which is a lower carbon abundance than CVs or CRs, but is isotopically similar to the CVs (Fig. 15).

The nitrogen isotope compositions of CR chondrites are characterized by heavy $\delta^{15}\text{N}$ values of ~ 100 to 190% (Ash and Pillinger 1995; Weisberg et al. 1995, and references therein; Pearson 2003). CV chondrites typically have lighter $\delta^{15}\text{N}$ values of ~ -9 to -45% (Kerridge 1985; Pearson 2003). The N isotope compositions of both NWA 1152 ($\delta^{15}\text{N} = -16.7\%$) and Sahara 00182 ($\delta^{15}\text{N} = -14.1\%$) suggest they are more similar to CV chondrites, although the N isotopic composition is likely to have been severely affected by desert weathering (Fig. 15).

Bulk Chemistry

Mg/Si ratios clearly indicate that NWA 1152 and Sahara 00182 are carbonaceous chondrites. In NWA 1152, atomic ratios of Al/Si are similar to literature values for CR, CI, and CH chondrites and Ca/Si ratios are more similar to literature values for CM, CO, CR, CI, and CH chondrites. In Sahara 00182 Al/Si ratios are most similar to CM and CO chondrites. Ca/Si ratios are higher than any known chondrite group, although this is likely to be caused by the high degree of terrestrial weathering seen in Sahara 00182 (Fig. 16).

SUMMARY AND PETROGENETIC IMPLICATIONS

Among the two samples Sahara 00182 is, perhaps, more similar to the CRs as traditionally recognized by their mineralogical and petrographic characteristics. For example, it is similar to CRs because of the high Fe-Ni metal content of chondrules and matrix, chondrule morphology and abundance, MgO-rich composition of olivine and pyroxene, the presence of silica-rimmed chondrules and the low abundance of refractory inclusions. However, it also shows a number of characteristics that are akin to the CV chondrites, for example, chondrule diameter, oxygen isotope composition, and the presence of Cr_2O_3 and FeO in spinel. The lack of phyllosilicates in chondrules and matrix and re-crystallized mesostasis indicates it is petrologic type 3.

NWA 1152 is perhaps more similar to the CVs, for example, in terms of metal abundance, lack of phyllosilicates, re-crystallized mesostasis, chondrule size, and nitrogen

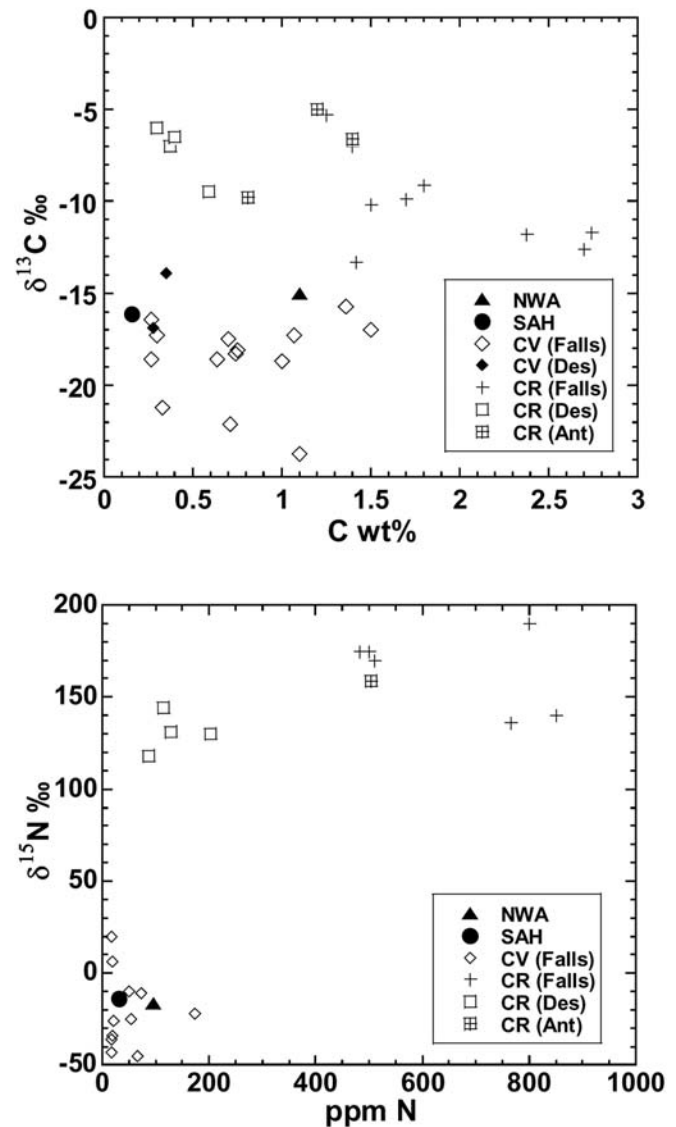


Fig. 15. Graphs of carbon and nitrogen abundance and isotopic composition in NWA 1152 and Sahara 00182 compared with CV and CR data. CV and CR carbon and nitrogen data from Kerridge (1985); Grady et al. (1991); Ash and Pillinger (1995); Weisberg et al. (1995) and Pearson (2003).

isotope composition. However, like Sahara 00182 it also displays characteristics that are indicative of a link with CR chondrites. The composition of olivine and pyroxene grains are extremely MgO-rich and display a restricted range, the sample has a high abundance of chondrules and chondrule fragments, contains very few refractory inclusions, and the Al/Si ratio is similar to the CRs. Importantly, both samples have oxygen isotope compositions that fall into the CV chondrite field as opposed to the CR chondrite field. Mineralogical, petrographic, isotopic, and bulk chemical data is summarized in Table 10.

On the basis of the discussions above, we feel that assigning these samples to a currently recognized

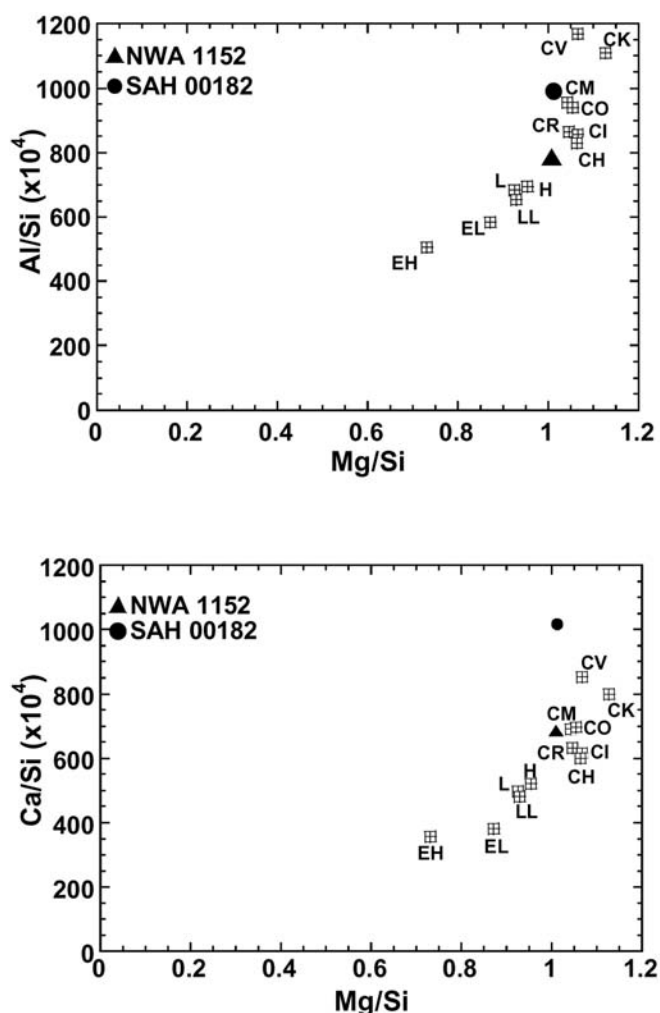


Fig. 16. Graphs of Mg/Si ratios versus Al/Si (top) and Ca/Si (bottom) for NWA 1152 and Sahara 00182 compared with literature values (from Table 6).

carbonaceous chondrite group is not yet possible. Although the oxygen isotope compositions suggest that both samples should be classed as CV chondrites, clear mineralogical, petrographic, and chemical differences exist with the CV chondrites as they are traditionally recognized.

In terms of many petrographic features (e.g., crystallinity of mesostasis, only slight olivine zonation, lack of observable phyllosilicates) it would certainly seem that both samples are type 3, with NWA 1152 showing evidence of higher degrees of thermal alteration. The mineralogical, petrographic, and compositional characteristics observed in chondrites are a combination of preserved original features and effects produced by secondary processes on the parent body, such as aqueous alteration and thermal metamorphism. Secondary processing in carbonaceous chondrites causes, for example, the presence of phyllosilicates in matrix, the oxidation of Fe-Ni metal to magnetite, and the equilibration of silicate minerals. However, some petrographic features will not be affected by secondary processing and, thus, will preserve the

original characteristics of the sample. For instance, the abundance, morphology, and size of chondrules will not be greatly changed by secondary alteration, although the composition may become equilibrated under conditions of thermal metamorphism. Similarly, although refractory inclusions may be altered through thermal or aqueous alteration, secondary processing will not change the abundance of inclusions in any given sample.

Considering the characteristics of NWA 1152 and Sahara 00182, as discussed above, it is apparent that they retain “original” features that are similar to, and imply a genetic link with the CR chondrites. Both samples have very low abundances of refractory inclusions, high abundances of chondrules and chondrule fragments, and MgO-rich silicate compositions—features all suggestive of CR grouping. However, the lack of phyllosilicates in both samples clearly indicates that they have not undergone the aqueous alteration typical of CR chondrites, although some alteration has occurred. Examples of alteration are the presence of sulfide and magnetite grains within the matrix, often surrounding grains of Fe-Ni metal, the presence of magnetite and sulfide veins associated with chondrules, and narrow fayalitic olivine rims around refractory inclusions. These alteration features are likely to have resulted from hydrothermal alteration and subsequent dehydration on the parent body (Krot et al. 1995, 1998) and in these respects they show similarities with the CV chondrites. The lack of zoning in olivine in NWA 1152 and the high-Ni content in matrix metal may suggest that this sample has undergone slightly more intense thermal alteration than Sahara 00182. Both samples show sulfidization of metal in chondrules and matrix (this is most clearly shown in Sahara 00182, which has a very high sulfide content, unlike any reported for the CV or CR chondrites) and could suggest redistribution of sulfur during parent body alteration.

Although NWA 1152 and Sahara 00182 apparently retain CR chondrite-like characteristics in terms of mineralogy and petrography, they have oxygen isotopic compositions that clearly fall into the CV field on an oxygen three-isotope plot (Fig. 5). Previous studies (e.g., Clayton et al. 1977; Clayton and Mayeda 1984, 1999; Clayton 1993) have suggested that variations in meteoritic oxygen isotope compositions are due to: 1) different materials having different and distinct isotopic compositions; and 2) geological processes occurring on different meteorite parent bodies. A combination of these two factors can account for the isotopic compositions (and variations in composition) observed in the carbonaceous chondrite groups. Carbonaceous chondrite groups fall into distinct regions on the oxygen three-isotope plot, a fact taken to suggest that the different groups formed on separate parent bodies with isotopically distinct oxygen isotope compositions and distinct geological histories. The oxygen isotopic composition of a sample is now commonly used for classification purposes, most notably for unusual or anomalous meteorite samples.

More recent studies have suggested that fluid flow on a

single chondritic parent body can account for the diversity in oxygen isotope composition (Bridges 1999; Young et al. 1999). Indeed, it has also been suggested (Young et al. 1999) that the mineralogy and petrography displayed by the CV, CM, and CI chondrites can also be accounted for by fluid flow on a single carbonaceous chondrite parent body. In this case, open system interactions between isotopically heavy fluid and lighter bulk rock will cause shifts in $\delta^{17}\text{O}$, $\delta^{18}\text{O}$, and $\Delta^{17}\text{O}$ to higher values in samples that have undergone higher degrees of aqueous alteration as indicated by the presence of phyllosilicates and carbonates.

The lack of a high abundance of phyllosilicates or pre-terrestrial carbonates in NWA 1152 and Sahara 00182 distinguishes them from the traditionally recognized CR chondrite samples and accounts for their petrologic type 3 classification. Therefore, it may be the case that NWA 1152, and especially Sahara 00182, represent a more primary CR-like material—they represent the composition and petrography of CR material prior to the onset of a significant aqueous alteration event(s). However, both samples have clearly undergone some aqueous/thermal alteration and it is probable that they represent CR-like material that has been thermally altered. For the CR chondrites and associated anhydrous meteorites (CH and CB chondrites), the oxygen isotopic compositions of CR, CH, and CB samples plot on or near the slope 0.7 “CR clan” line (Weisberg et al. 1995) (Fig. 5). Thus, if indeed NWA 1152 and Sahara 00182 represent anhydrous CRs (CR3s) then, we may expect them to plot in an extension of this oxygen three-isotope field. However, Fig. 5 shows them both clearly falling within the CV field.

If NWA 1152 and Sahara 00182 do indeed represent primary (i.e., pre-accretion with subsequent aqueous alteration) CR material, then this material must have had some affinity with the CV chondrites, in that they have very similar oxygen isotopic compositions. However, anhydrous minerals from CR chondrites do not have CV-like oxygen isotopic compositions (Weisberg et al. 1993, 1995; Clayton and Mayeda 1999). Furthermore, the lack of refractory inclusions, chondrule abundance, and differences in chemistry indicates that the CRs cannot simply be aqueously altered CV material and, conversely, that CVs are not simply thermally metamorphosed and dehydrated CRs.

Mineralogical, petrographic, and oxygen isotope data seem to be inconsistent, suggesting that assignment of NWA 1152 and Sahara 00182 into any one of the currently known carbonaceous chondrites classes might be an oversimplification. Both NWA 1152 and Sahara 00182 demonstrate the complexity of relationships among and between the carbonaceous chondrites. Studies of the least altered carbonaceous chondrites demonstrate the difficulties of categorizing meteorites into a small number of groups that are assumed to share a common asteroidal parent body. Instead, our meteorite collections may sample many small asteroids that share some compositional similarities and

genetic affinities. Whatever the classification of NWA 1152 and Sahara 00182, these two meteorites clearly represent a new source of relatively pristine solar system material.

Acknowledgments—Caroline Smith was funded by PPARC during this study. The Carnegie Trust for the Universities of Scotland is thanked for providing funds for color images. The authors would like to thank Robert Hutchison for helpful comments and suggestions during this study. Jenny Gibson and Sasha Verchovsky (Open University) are kindly thanked for assisting with C and N isotope analyses. Sarah James (NHM) is thanked for assisting with chemistry and ICP-AES analyses. The authors sincerely thank Sasha Krot and Michael Weisberg for reviews that were extremely helpful and improved the manuscript. The authors would also like to thank Associate Editor Hiroko Nagahara for helpful comments.

Editorial Handling—Dr. Hiroko Nagahara

REFERENCES

- Anders E. and Grevesse N. 1989. Abundances of the elements: Meteoritic and solar. *Geochimica et Cosmochimica Acta* 53:197–214.
- Ash R. D. and Pillinger C. T. 1995. Carbon, nitrogen, and hydrogen in Saharan chondrites: The importance of weathering. *Meteoritics* 30:85–92.
- Bischoff A., Palme H., Ash R. D., Clayton R. N., Schultz L., Herpers U., Stöffler D., Grady M. M., Pillinger C. T., Spettel B., Weber H., Grund T., Endreß M., and Weber D. 1993. Paired Renazzo-type (CR) carbonaceous chondrites from the Sahara. *Geochimica et Cosmochimica Acta* 57:1587–1603.
- Brearley A. J. and Jones R. H. 1998. Chondritic meteorites. In *Planetary materials*, edited by Papike J. J. Washington D.C.: Mineralogical Society of America. pp. 3–1–3–398.
- Bridges J. C. 1999. Mineralogical controls on the oxygen isotopic compositions of UOCs. *Geochimica et Cosmochimica Acta* 63: 945–951.
- Chizmadia L. J., Rubin A. E., and Wasson J. T. 2002. Mineralogy and petrology of amoeboid olivine inclusions in CO3 chondrites: Relationship to parent body aqueous alteration. *Meteoritics & Planetary Science* 37:1781–1796.
- Clayton R. N. 1993. Oxygen isotopes in meteorites. *Annual Review of Earth and Planetary Sciences* 21:115–149.
- Clayton R. N. and Mayeda T. K. 1984. The oxygen isotope record in Murchison and other carbonaceous chondrites. *Earth and Planetary Science Letters* 67:151–166.
- Clayton R. N., Onuma N., Grossman L., and Mayeda T. K. 1977. Distribution of the presolar component in Allende and other carbonaceous chondrites. *Earth and Planetary Science Letters* 34:209–224.
- Clayton R. N. and Mayeda T. K. 1999. Oxygen isotope studies of carbonaceous chondrites. *Geochimica et Cosmochimica Acta* 63: 2089–2104.
- Connolly H. C. Jr., Huss G. R., and Wasserburg G. J. 2001. On the formation of Fe-Ni metal in Renazzo-like carbonaceous chondrites. *Geochimica et Cosmochimica Acta* 65:4567–4588.
- Fuchs L. H. and Olsen E. 1973. Composition of metal in type III carbonaceous chondrites and its relevance to the source-

- assignment of Lunar metal. *Earth and Planetary Science Letters* 18:379–384.
- Grady M. M., Wright I. P., and Pillinger C. T. 1991. Comparisons between Antarctic and non-Antarctic meteorites based on carbon isotope geochemistry. *Geochimica et Cosmochimica Acta* 55:49–58.
- Grady M. M., Verchovsky A. B., Franchi I. A., Wright I. P., and Pillinger C. T. 2002. Light element geochemistry of the Tagish Lake CI2 chondrite: Comparison with CI1 and CM2 meteorites. *Meteoritics & Planetary Science* 37:713–735.
- Greenwood R. C., Lee M. R., Hutchison R., and Barber D. J. 1994. Formation and alteration of CAIs in Cold Bokkeveld (CM2) *Geochimica et Cosmochimica Acta* 58:1913–1935.
- Grossman J. N. and Zipfel J. 2001. The Meteoritical Bulletin, No. 85. *Meteoritics & Planetary Science* 36:A293–A322.
- Grossman J. N., Rubin A. E., Nagahara H., and King E. A. 1988. Properties of chondrules. In *Meteorites and the early solar system*, edited by Kerridge J. F. and Matthews M. S. Tucson: The University of Arizona Press. pp. 619–659.
- Ikeda Y. and Kimura M. 1995. Anhydrous alteration of Allende chondrules in the solar nebula, I. Description and alteration of chondrules with known oxygen isotopic compositions. *Proceedings of the NIPR Symposium on Antarctic Meteorites* 8: 97–122.
- Jarosewich E., Clarke R., and Barrows J. S. 1987. The Allende meteorite reference sample. *Smithsonian Contributions to Earth Sciences* 27.
- Kallemeyn G. W. and Wasson J. T. 1991. The compositional classification of chondrites, V. The Karoonda (CK) group of carbonaceous chondrites. *Geochimica et Cosmochimica Acta* 55: 881–892.
- Kallemeyn G. W., Rubin A. E., and Wasson J. T. 1994. The compositional classification of chondrites, VI. The CR carbonaceous chondrite group. *Geochimica et Cosmochimica Acta* 58:2873–2888.
- Kerridge J. F. 1985. Carbon, hydrogen, and nitrogen in carbonaceous chondrites: Abundances and isotopic compositions in bulk samples. *Geochimica et Cosmochimica Acta* 49:1707–1714.
- Kimura M. and Ikeda Y. 1995. Anhydrous alteration of Allende chondrules in the solar nebula, I. Alkali-Ca exchange reactions and formation of nepheline, sodalite, and Ca-rich phases in chondrules. *Proceedings of the NIPR Symposium on Antarctic Meteorites* 8:123–138.
- Krot A. N., Scott E. R. D., and Zolensky M. E. 1995. Mineralogical and chemical modification of components in CV3 chondrites: Nebular or asteroidal processing? *Meteoritics* 30:748–775.
- Krot A. N., Scott E. R. D., and Zolensky M. E. 1997. Origin of fayalitic olivine rims and lath-shaped matrix olivine in the CV3 chondrite Allende and its dark inclusions. *Meteoritics & Planetary Science* 32:31–49.
- Krot A. N., Pataev M. I., Scott E. R. D., Choi B. G., Zolensky M. E., and Keil K. 1998. Progressive alteration in CV3 chondrites: More evidence for asteroidal alteration. *Meteoritics & Planetary Science* 33:1065–1085.
- Krot A. N., Meibom A., Weisberg M. K., and Keil K. 2002. The CR chondrite clan: Implications for early solar system processes. *Meteoritics & Planetary Science* 37:1451–1490.
- Lee M. R. and Greenwood R. C. 1994. Alteration of calcium and aluminium-rich inclusions in the Murray (CM2) carbonaceous chondrite. *Meteoritics* 29:780–790.
- Macpherson G. J., Wark D. A., and Armstrong J. T. 1988. Primitive material surviving in chondrites: Refractory inclusions. In *Meteorites and the early solar system*, edited by Kerridge J. F. and Matthews M. S. Tucson: The University of Arizona Press. pp. 746–807.
- Mason B. and Wiik H. B. 1962a. Descriptions of two meteorites: Karoonda and Erakot. *American Museum Novitates* 2106.
- Mason B. and Wiik H. B. 1962b. The Renazzo meteorite. *American Museum Novitates* 2115.
- McSween H. Y., Jr. 1977. Petrographic variations among carbonaceous chondrites of the Vigarano type. *Geochimica et Cosmochimica Acta* 41:1977–1790.
- McSween H. Y., Jr. and Richardson S. M. 1977. The composition of carbonaceous chondrite matrix. *Geochimica et Cosmochimica Acta* 41:1145–1161.
- Miller M. F., Franchi I. A., Sexton A. S., and Pillinger C. T. 1999. High precision $\delta^{17}\text{O}$ measurements of oxygen from silicates and other oxides: Method and applications. *Rapid Communication in Mass Spectrometry* 13:1211–1217.
- Mittlefehldt D. W. 2002. Geochemistry of the ungrouped carbonaceous chondrite Tagish Lake, the anomalous CM chondrite Bells, and comparison with CI and CM chondrites. *Meteoritics & Planetary Science* 37:703–712.
- Murakami T. and Ikeda Y. 1994. Petrology and mineralogy of the Yamato-86751 CV3 chondrite. *Meteoritics* 29:397–409.
- Newton J., Bischoff A., Arden J. W., Franchi I. A., Geiger T., Greshake A., and Pillinger C. T. 1995. Acfer 094, a uniquely primitive carbonaceous chondrite from the Sahara. *Meteoritics* 30:47–56.
- Pearson V. K. 2003. Organic-inorganic relationships in the carbonaceous chondrites. Ph.D. thesis, The Open University, Milton Keynes, Bucks, UK.
- Rubin A. E. 2000. Petrologic, geochemical, and experimental constraints on models of chondrule formation. *Earth Science Reviews* 50:3–27.
- Russell S. S., Davis A. M., Macpherson G. J., Guan Y., and Huss G. R. 2000. Refractory inclusions from the ungrouped carbonaceous chondrites MAC 87300 and MAC 88107. *Meteoritics & Planetary Science* 35:1051–1066.
- Scott E. R. D. 1988. A new kind of primitive chondrite, Alan Hills 85085. *Earth and Planetary Science Letters* 91:1–18.
- Simon S. B., Grossman L., Casanova I., Symes S., Benoit P., Sears D. W. G., and Wacker J. F. 1995. Axtell, a new CV3 chondrite find from Texas. *Meteoritics* 30:42–46.
- Smith C. L. 2002. An integrated mineralogical, petrologic, and isotopic study of ureilites. Ph.D. thesis, The Open University, Milton Keynes, Bucks, UK.
- Tomeoka K., McSween H. Y., Jr., and Buseck P. R. 1989. Mineralogical alteration of CM carbonaceous chondrites: A review. *Proceedings of the NIPR Symposium on Antarctic Meteorites* 2:221–234.
- Thompson M. and Walsh J. N. 1983. *A handbook of inductively coupled plasma spectrometry*. London: Blackie and Son. pp. 84–85.
- Van Schmus W. R. and Wood J. A. 1967. A chemical-petrologic classification for the chondritic meteorites. *Geochimica et Cosmochimica Acta* 31:747–765.
- Verchovsky A. B., Fisenko A. V., Semjonova L. F., and Pillinger C. T. 1997. Heterogeneous distribution of xenon-HL within presolar diamonds. *Meteoritics & Planetary Science* 32:131–132.
- Verchovsky A. B., Fisenko A. V., Semjonova L. F., Wright I. P., Lee M. R., and Pillinger C. T. 1998. C, N, and noble gas isotopes in grain size separates of presolar diamonds from Efremovka. *Science* 281:1165–1168.
- Wasson J. T. and Kallemeyn G. W. 1988. Composition of chondrites. *Philosophical Transactions of the Royal Society of London A* 325:535–544.

- Wasson J. T. and Kallemeyn G. W. 1990. Allan Hills 85085: A subchondritic meteorite of mixed nebular and megalithic heritage. *Earth and Planetary Science Letters* 101:148–161.
- Weber D. and Bischoff A. 1997. Refractory inclusions in the CR chondrite Acfer 059–El Djouf 001: Petrology, chemical composition, and relationship to inclusion populations in other types of carbonaceous chondrites. *Chemie der Erde* 57:1–24.
- Weisberg M. K. 2001. Sahara 00182, the first CR3 chondrite and formation of multi-layered chondrules (abstract). *Meteoritics & Planetary Science* 36:A222.
- Weisberg M. K., Prinz M., Clayton R. N., and Mayeda T. K. 1993. The CR (Renazzo-type) carbonaceous chondrite group and its implications. *Geochimica et Cosmochimica Acta* 57:1567–1586.
- Weisberg M. K., Prinz M., Clayton R. N., Mayeda T. K., Grady M. M., and Pillinger C. T. 1995. The CR chondrite clan. *Proceedings of the NIPR Symposium on Antarctic Meteorites* 8:11–32.
- Wlotzka F. 1993. A weathering scale for the ordinary chondrites. *Meteoritics* 28:460.
- Young E. D. and Russell S. S. 1998. Oxygen reservoirs in the early solar system inferred from an Allende CAI. *Science* 282:452–455.
- Young E. D., Ash R. D., England P., and Rumble D., III. 1999. Fluid flow in chondritic parent bodies: Deciphering the compositions of planetesimals. *Science* 286:1331–1335.
- Zolensky M. E., Barrett R., and Browning L. 1993. Mineralogy and composition of matrix and chondrule rims in carbonaceous chondrites. *Geochimica et Cosmochimica Acta* 57:3123–3148.
- Zolensky M. E., Nakamura K., Gounelle M., Mikouchi T., Kasama T., Tachikawa O., and Tonui E. 2002. Mineralogy of Tagish Lake: An ungrouped type 2 carbonaceous chondrite. *Meteoritics & Planetary Science* 37:737–761.
-